OPTIMISATION OF THE OXYGEN DIFFUSION PROCESS FOR SURFACE HARDENING OF THE Ti-6Al-4V ALLOY

A thesis submitted to the Faculty of Engineering and the Built environment, University of Cape Town, in fulfilment of the requirements for the degree of Master of Science in Engineering.

By

Liezl Anne Matthews

Department of Mechanical Engineering

October 2008

ABSTRACT

Titanium-6Al-4V is a widely used engineering material, utilised in the aerospace industry due to attractive properties such as high strength to weight ratio and excellent corrosion resistance. However poor tribological properties are inherent to titanium alloys and surface modification processes are thus used to engineer surface hardening.

A well established method of surface hardening for titanium alloys is through solid solution strengthening by alloying with oxygen. This is achieved through a two step oxygen boost diffusion hardening (OBDH) process. During the oxidation step, the formation of a thick adherent rutile TiO_2 layer occurs which is followed by subsequent boost diffusion (step 2) wherein the oxide layer is decomposed to free up oxygen for boost diffusion hardening.

Step 1 is characteristically conducted at 850^{o}C for 30 minutes in an oxygen rich environment followed by cooling. Step 2 is conducted in an oxygen free environment at 850^{o}C for 20 hours. The approach of the present study was to refine the OBDH process and gain understanding of the mechanism responsible for boost diffusion hardening in order to optimise boost diffusion hardening. This was done by introducing and comparing the hardening results for a cyclic isothermal OBDH treatment and a continuous thermal OBDH treatment to the resultant hardening of the original two step process which included cooling after step 1. The cyclic isothermal treatment achieved optimum boost diffusion hardening in the shortest amount of treatment time.

A combination of scanning electron microscopy (SEM) and electron backscattered diffraction (EBSD) analysis has been utilised to examine the nature of the oxide/metal interface and surrounding grain structures as a result of the OBDH process. These images showed that oxide formation occurs through a nucleation and growth mechanism during step 1, as well as the transformation of TiO_2 into new titanium metal at the interface due to decomposition of the oxide layer during step 2. These images revealed the grain structural evolution during the OBDH process which clarified the boost diffusion mechanism.

DECLARATION

I know the meaning of plagiarism and declare that all the work in the document, save for that which is properly acknowledged, is my own.

Signed:

Liezl Anne Matthews

October 2008

ACKNOWLEDGEMENTS

I would like to thank everyone who has assisted me throughout the duration of this project, particularly towards the end of it:

Advance Manufacturing Technology Strategy (AMTS) for providing financial support for this project.

The National Metrology Institute of South Africa (NMISA) for the use of their scanning electron microscope.

The Physics Department at the Nelson Mandela Metropolitan University (NMMU) for the use of their Nanoindenter.

My supervisor Professor Rob Knutsen, for his encouragement, supervision and guidance.

Miss Sarah Louise George, who without fail, will have a good answer to any question or at least know where to find it.

Mrs Penelope Park-Ross for emotional and technical support in the laboratory.

Mr Glen Newins and the workshop staff for all technical support from high precision machining to changing tyres.

All students and staff at the Centre for Materials Engineering for their support and assistance.

Family and friends for their continual support, understanding and prayer.

TABLE OF CONTENTS

LIST OF FIGURES

LIST OF TABLES

1 INTRODUCTION

Titanium-6Al-4V has excellent corrosion resistance and high strength to weight ratio and is an attractive engineering material for utilisation in the aerospace and automotive industries. Titanium alloys have inherent poor tribological properties which lower their mechanical performance[1,2,3,4,5,6,7,8]. These properties can be improved through a number of surface modification processes which engineer increased surface hardness. A well established and reported method of surface modification is the alloying of titanium alloys with oxygen[1,2,3,4,5,6,7,8]. Oxygen atoms dissolve in solid solution, into the α/β microstructure, stabilise the hexagonal close-packed (hcp) α-phase and cause concomitant increase in resistance to dislocation movement which causes an increase in surface hardness. Effective hardening of the titanium alloy substrate is achieved through a combination of thermal oxidation and oxygen diffusion movement into the substrate and is known as oxygen boost diffusion hardening (OBDH)[1,4,5]. Hardening is achieved during this process through the formation of an adherent oxide layer of optimum thickness on the alloy surface. This layer subsequently decomposes to release oxygen which diffuses into the substrate causing interstitial solid solution. In this process the oxide layer serves as the oxygen reservoir for the boost diffusion process. OBDH is thus achieved by the initial formation of an oxide layer in an oxygen rich environment, followed by the decomposition of the oxide layer in an oxygen free environment.

A two step thermal process is conducted at temperatures above 600^{o}C in order to perform effective OBDH of the Ti-6Al-4V alloy. The typical temperature range is between 750-850^{o}C[3,4,6,7]. The time required for the formation of an adherent oxide layer (step 1) is 30 minutes while the decomposition of the oxide layer (step 2) to achieve adequate OBDH is 20 hours.

Several arguments are proposed in this thesis to further optimise the OBDH process.
(i) It can be argued that the discontinuous 2 step process leads to some level of disruption of the oxide-metal interface during cooling and re-heating between steps. On the other hand the disruption occurs at the interface during the cooling process due to the differential thermal contraction between the oxide layer and the titanium alloy

substrate. Hence it may be hypothesised that continuous isothermal treatments will produce more effective boost diffusion hardening than conventional two step treatments that involve cooling to room temperature after step 1. The reason for this is that high interface quality can be maintained during the continuous isothermal treatments.

(ii) Cyclic isothermal treatments which cycle between the oxidation and boost diffusion steps could further refine the OBDH process. It is speculated that the cyclic treatments will produce greater hardening than conventional two step treatments. This anticipated behaviour results from the fact that greater oxide reservoirs will be accumulated in the incremental oxidation steps due to the parabolic growth rate of the oxide layer than the reservoirs accumulated in the conventional process. The interrupted oxide growth, during the shorter growth times, will result in less strain at the interface as opposed to the strain caused by a larger increase oxide layer volume due to thickness at the interface of an oxide layer formed during a continuous oxidation step. This thinner oxide layer will maintain interface integrity which is crucial for the oxygen boost diffusion movement during step 2. If boost diffusion could be enhanced through these modified treatments, shorter boost diffusion times could be used which would allow less grain growth over the total thermal cycle.

(iii) A high vacuum boost diffusion step and an inert gas environment (argon) boost diffusion step could achieve similar hardening results since both environments are free of oxygen. Consequently, no oxygen is available at the oxide surface to diffuse through the oxide layer and into the substrate.

(iv) The boost diffusion hardening results of OBDH treatments that included oxidation in pure oxygen were compared to those of treatments that included oxidation in medical air, containing 21% O_2 and 79% N, to determine the influence of nitrogen during the oxidation step on the boost diffusion movement of oxygen.

As a consequence of the experiments that evolved to address the arguments mentioned above, insight was gained into the finer details of the mechanism of the OBDH process. This aspect is emphasised in the presentation of the results and discussion.

2 LITERATURE REVIEW

2.1 Titanium

2.1.1 Material introduction

Titanium is a widely used engineering material due to its good formability, high strength to weight ratio and its excellent corrosion resistance properties[9]. Commercially pure grades of titanium have a range of yield strengths (170 MPa – 480 MPa)[20]. Titanium is used widely in biomedical applications for both orthopaedic and dental implants[10] as well as in the automotive and aerospace industries[8].

Titanium is a highly reactive metal and reacts readily with interstitial elements such as oxygen, carbon, nitrogen and hydrogen[8,28]. Titanium is a transition metal which implies that it can form solid solutions with substitutional elements with similar size factors within ±20 %[8]. The formation of a self protective passive oxide layer composed of amorphous or low crystalline titanium oxide (TiO_2) occurs during the reaction between titanium and oxygen at room temperature. This transparent layer protects the underlying metal from further oxidation resulting in the very high corrosion resistance of titanium even under marine conditions[8,10, 11,14,16,12,13,30,32].

Titanium is considered to have very good biocompatibility[14,15,16,30]. However, its biocompatibility is compromised by poor tribological properties[17,28], which due to the low wear resistance of titanium alloys, produces wear debris which can result in adverse response of the tissue surrounding the orthopaedic joints[1,18].

2.1.2 Processing

The cost of converting titanium dioxide (TiO_2) into commercially pure titanium is very high. Since the 1940's the known process has been the prevailing Kroll process, during which TiO_2 is converted into titanium sponge which is melted and cast. This is a complicated, lengthy and high energy consuming process making it costly, as at melting temperatures, above 1650^{o}C, titanium is highly reactive[19]. Production processes have therefore been developed to try to convert TiO_2 directly into metallic

titanium. Many of these processes have been unsuccessful in supplying the required energy to remove interstitially dissolved oxygen, as more oxygen is removed, the affinity of the titanium for oxygen increases, increasing the amount of energy required by the reducing agent. Some successful methods, such as the Fray-Farthing-Chen (FFC) Cambridge method have been developed[9]. In spite of developments processing and machining costs for titanium remain high compared to that of aluminium and steel[8]. The performance benefits of replacing aluminium or steel with titanium for a specific application must, therefore, markedly outweigh the costs.

2.1.3 Use in the aerospace industry

From as early as 1952, titanium alloys have been used in the aerospace industry as compressor blades and disks in gas turbines[8]. Today titanium alloys are used for the manufacture of a wide range of commercial aircraft components. Titanium alloys, compared to aluminium and steel, are more compatible with the carbon composites used for the manufacture of certain aircraft components[9]. Weight savings are achieved by replacing steel with titanium for the production of high pressure hydraulic tubing. Titanium alloy components can withstand higher operating temperatures than most aluminium alloys, which can only operate at temperatures below 130^{o}C, such as are experienced in the environmental control systems in commercial aircraft which operate at 230^{o}C. Landing gear components need to have critical load carrying capacity while complying with dimension constraints, for which titanium alloys are utilised.

Metal coating and painting is used to prevent corrosion of aircraft components. Titanium alloys, however, have sufficient corrosion resistance to be used uncovered in corrosive environments. Titanium alloy components are only coated when they are used alongside a dissimilar metal and galvanic corrosion attack can occur[20].

2.1.4 Titanium alloy types

Three types of titanium alloy types exist according to their phase composition at room temperature. These alloys are classified as α and near α alloys (referred to as α alloys), α/β alloys (sometimes referred to as α+β alloys) and β alloys[8].

Each type of alloy is suited to specific applications: α alloys are suited to high temperature applications - up to 540°C for dynamic and 565°C for static components. Above these temperatures for the different components the danger arises that titanium will react with oxygen in the air and thereby reducing the ductility and fatigue strength of the material. β alloys are well suited in high strength applications which require high corrosion resistance. These β titanium alloys continue thinning after necking thus exhibiting no work hardening and are extensively used for spring manufacturing.

Superior corrosion resistance and weight reduction is exhibited by α/β alloys such as the Ti-6Al-4V alloy. The strength and fracture toughness of these alloys can be altered through heat treatments. These treatments have to be conducted under high vacuum conditions to prevent surface reactions between titanium alloys and elements such as oxygen, nitrogen and hydrogen that result in the formation of a brittle surface layer[33].

2.1.5 Titanium-6Al-4V

This alloy is known as the workhorse of the titanium family and accounts for 60% of the annual world tonnage production of titanium and titanium alloys[21]. This alloy is most extensively used in the aerospace industry accounting for 80% - 90% of applications[20]. It consists of 6 weight percent aluminium and 4 weight percent vanadium. The following table shows the alloying composition of Ti-6Al-4V:

Alloying element	**Ti**	**Al**	**V**	**Fe**	**O**
Weight percentage	90	6	4	0.25 Max	0.2 Max

Table 1: Alloying composition of Ti-6Al-4V[22,23].

The wide range of uses is result of its favourable properties in both engineering and medical applications. The following table shows some of the material properties of Ti-6Al-4V.

Mechanical properties	Elongation at break (%)	< 10
	Modulus of elasticity (GPa)	106 – 114
	Tensile strength (MPa)	896 – 1410
	Fracture Toughness (MPa√m)	66 - 88
	Hardness (Vickers)	349
	Fatigue Strength (Mpa)	510
	Shear Modulus (GPa)	44
Physical properties	Density (g cm^{-3})	4.42-4.43
	Melting point (^oC)	1600 – 1650
	β Transus (^oC)	980
Thermal properties	Coefficient of thermal expansion (x 10^{-6} K^{-1})	8 @ 20 – 100^oC
	Thermal conductivity (W m^{-1} K^{-1})	5.8 @ 23^oC

Table 2: Material properties of Ti-6Al-4V[20,22,23].

2.1.6 Microstructural changes due to temperature change

Ti-6Al-4V is an α/β alloy containing α with a hexagon close-packed (hcp) crystal structure, and β with a body centred cubic (bcc) structure at room temperature. Aluminium is an α phase stabiliser while vanadium is a β phase stabiliser. When an α/β alloy is heated above the α/β transition temperature all the material is in the β phase. the α/β transition temperature (980^oC) is therefore raised by the addition of aluminium and lowered by the addition of vanadium. The following diagram illustrates the influence of β-titanium stabilizer on the phase composition.

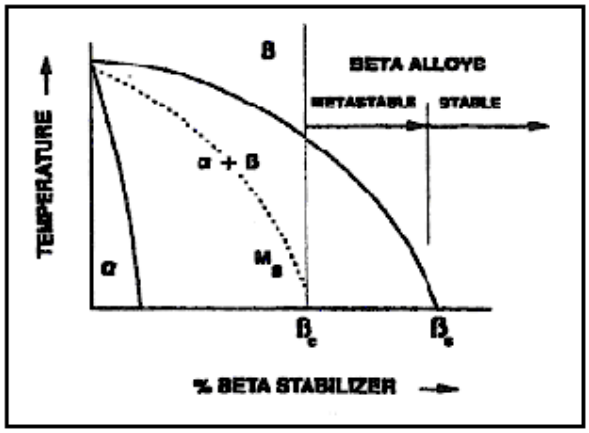

Figure 1: Pseudo-binary phase diagram illustrating the influence of percentage β-titanium stabiliser[8].

When controlled amounts of stabilisers for both α and β phases are present in the alloy both phases are present at room temperature, and it is assumed that aluminium will be present in the α crystals and vanadium in the β crystals[8]. The following diagram shows the annealed microstructure of the Ti-6Al-4V alloy in the α/β phase condition at room temperature. The α phase is seen as the light grains surrounded by the darker β phase. The microstructure consists of 90% α grains and 10% β grains.

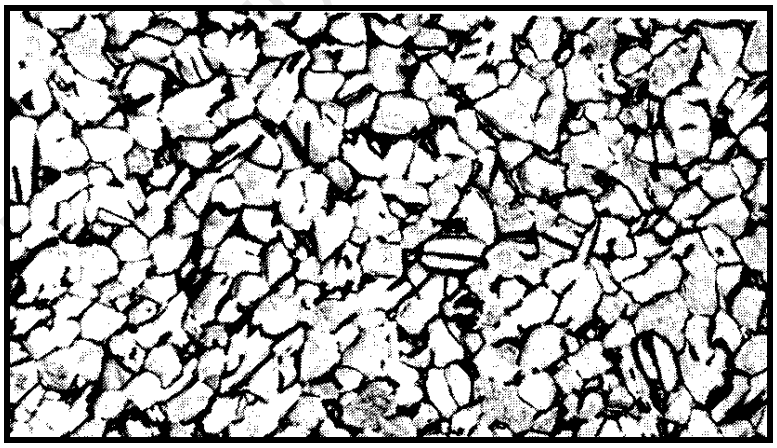

Figure 2: The α/β microstructure composition at room temperature of annealed Ti-6Al-4V[24].

When α/β alloys are heated to temperatures above the β transus and cooled, two transformations are known to occur. The first is the development of Widmanstätten

growth, which consists of long parallel plates of α surrounded by thin layers of β. The α plates grow parallel to the [1, $\bar{1}$, 0] plane of the β grains. As there are six sets of non-parallel planes in a given β grain, sets of α plates are formed in six non-parallel directions[25]. This α-plate growth occurs for all practical cooling rates from the β transus although coarser structures are formed at lower furnace cooling rates[25].

The second transformation is martensite formation. This is formed when specimens are quenched from above β transus. The β now transforms into α' (α prime) which has a supersaturated hcp α crystal structure[26]. During the OBDH process the treatment temperature (600-900^{o}C) is never above that of the β transus and these transformations do not occur. However, when an annealed α/β alloy is treated at a temperature range of 600-900^{o}C grain growth for both phases is expected.

2.2 Surface hardening

2.2.1 Surface reaction layers

Titanium alloys have relatively low shear strength, high friction coefficients and are prone to undergo adhesive wear at joints[27]. Traditional lubricants are often ineffective for titanium wear applications and surface treatments such as anodizing and electroplating can only withstand light wear loads[8]. Many surface hardening methods have therefore been developed to improve the inherent poor tribological properties of titanium alloys[13,28].

Cai et al[29] found a 150 – 200 μm thick reaction layer on the surface of investment cast titanium which had, compared to the underlying metal, increased hardness as well as reduced elongation. This layer was said to form due to the high reactivity of titanium at elevated temperatures that would cause the titanium to react with elements such as oxygen, nitrogen and carbon in the investment. These elements were extracted out of oxides in the investment and diffused into the titanium creating the reaction layer. These atoms locate themselves in interstitial positions in the titanium microstructure. This reduction of other oxides occurred because titanium has very strong reducing power which causes the decomposition of oxides common to investments such as MgO and Al_2O_3[30]. Different investment materials that are more thermodynamically

stable than titanium oxide were used in order to limit the formation of this reaction layer, as these reaction layers inhibit the strong bonding between casting and dental porcelain making it unsuitable for dentistry[30].

A hardened surface layer similar to the reaction layer on investment cast titanium alloys is suitable in applications where components experience wear. Many methods have been designed to use the reactive property of titanium to improve surface hardness. Surface hardening of the alloy surface can be engineered by introducing coatings through plasma glow spray, plasma nitriding, chemical vapour deposition (CVD) or physical vapour deposition (PVD), and even electrochemical processes such as spark anodizing[31].

2.2.2 Thermal oxidation of titanium

Surface modification of titanium alloys can be achieved by thermal oxidation in air at elevated temperatures either under radiant heat furnace conditions or through glow discharge[32]. The formation of an oxide layer occurs on the surface of the material which is often thick, with unsatisfactory adhesion to the substrate. The material immediately underneath the oxide layer has oxygen and nitrogen atoms diffused into the lattice interstitially causing solid solution strengthening of this region. Hardening of titanium through thermal oxidation treatments has been successfully achieved with high increases in hardness close to the surface reported after 60 hours at 600 ^{o}C[2]. By adjusting treatment time and temperature, the adhesion to the metal and the thickness of the oxide layer, as well as the hardening of the diffused region can be controlled[28]. By increasing the time and temperature the hardening can be increased but at the same time the oxide layer thickness increases, causing stratification of the oxide layer and delamination of the oxide layer from the metal. Oxide layer scaling severely damages the surface integrity of the material and thereby limiting the use of this treatment for surface hardening of titanium. Required surface quality therefore, limits the achievable hardening during thermal oxidation of titanium alloys.

A novel method of boost diffusion hardening exists in which a adherent oxide layer is found on the surface with a boost diffusion hardened zone underneath. This method has been found to greatly improve the tribological properties of titanium alloys. This

method is a two step process of which step 1 is a thermal oxidation step followed by a boost diffusion step (step 2). This method results in better surface integrity while increasing the depth and magnitude of the hardening in the underlying metal.

2.2.3 Oxygen boost diffusion hardening (OBDH)

Boost diffusion hardening of Ti-6Al-4V and its alloys can be achieved through alloying in oxygen rich environments at temperatures in excess of 600^{o}C[33]. Luo et al[5] suggest that the high affinity of titanium for oxygen is shown by the similarities in the bond energies between Ti-Ti bonds and Ti-O bonds. The energies are given as 2.12 eV and 2.56 eV respectively for each bond to form.

Oxygen is introduced through the two step process: an oxidation step in which an adherent oxide layer of optimum thickness forms on the metal surface followed by a boost diffusion step during which oxygen from the oxide layer diffuses into the metal increasing the diffusion hardening that occurred during the oxidation step as well as increasing the depth of hardening. The apparent discontinuity between the two solid layers (oxide and metal) is referred to as the interface from here onwards.

2.2.3.1 Step 1: Oxidation

This step is conducted in an oxygen rich environment at elevated temperature. Two important processes occur simultaneously during the oxidation step namely: oxide formation and interstitial solid solution strengthening of titanium metal. Both these processes occur through the continual diffusion movement of oxygen atoms into the metal.

Zhang et al[3] found a high rate of oxygen accumulation exists at temperatures between 800^{o}C-900^{o}C, during which a reddish brown oxide layer was formed. The rate of oxygen accumulation is higher at 850^{o}C than at 800^{o}C, shown by increased weight gain at the higher temperature. The weight gain for a specimen oxidised at 850^{o}C for 20 minutes was 0.7642 mg/cm^{2} while 0.661 mg/cm^{2} for oxidation at 800^{o}C for 60 minutes. Lenarduzzi et al[7] found that the mass gain measured for oxidised specimens increased as the oxygen concentration in the oxidising medium increased.

Dong et al[4] found that the optimal treatment temperature for the oxidation step to be 850°C and that the weight gain during oxidation at this temperature had a linear relationship with treatment time. They conducted oxidation experiments for 16, 30, 45 and 60 minutes at 850°C during which time a dark brown oxide layer had formed on all these specimens. They stated that during the optimum oxidation treatment the weight gain for the specimen is less than 1 mg/cm^2 which they found occurs at an oxidising temperature of 850°C for 30 minutes or less.

2.2.3.1.1 Oxide formation during the oxidation step

Two schools of thought existed around the oxide formation: some suggested that titanium atoms move to the surface to form TiO_2 causing outward oxide growth, while others offered that oxygen atoms diffuse into the metal causing the oxide layer to grow inwards. Generally it is now believed that oxide formation occurs into the metal as the microstructure defects which would restrict Ti migration, would allow oxygen diffusion movement[5].

During the oxidation step, through oxygen diffusion movement, the oxygen concentration at the metal surface will reach stoichiometry (33, 4 weight % or 66,67 atomic %) to form rutile titanium oxide ($TiO_{2.}$)[5]. The transformation of titanium to oxide occurs in titanium metal with stoichiometric solid solution oxygen concentrations. The oxygen concentration will decrease, as the distance from the surface increases, following the parabolic shape[7] of the concentration gradient. Some authors suggest that the oxygen concentration growth profile during oxide formation is parabolic as the oxide layer initially is compact after which a linear growth rate is followed which results in the formation of a thick lamellar oxide layer[5], while others suggest that the oxide growth follows a linear growth rate at a very early stage after the parabolic growth stage[4].

The oxidation step in this process has been characteristically conducted at temperatures ranging from 600 – 900°C[6, 7] for differing amounts of time. In this temperature range thermodynamically stable rutile TiO_2 can form. The thickness of this layer can be controlled through treatment temperature and time. Dong et al[4] found that a specimen oxidised at 850°C for 20.5 hours had a flaky white oxide layer

in which stratification causing many sub layers, occurred. Lenarduzzi et al[7] found that after oxidation experiments conducted at 850°C for 30 minutes two forms of TiO_2 were present: rutile and anatase which are both tetragonal but have different structures. In rutile the structure is based on octahedrons of titanium oxide which share two edges of the octahedron, while in anatase, the octahedrons share four edges. They also expected that Brookite (orthorhombic) could be present as it is another polymorphic component of rutile. They stated that with a rise in temperature in Ti-O systems the following transformations will occur: Anatase → Rutile → Brookite → liquid. These findings are inconsistent with those of Luo et al[5] who report that only rutile TiO_2 forms at treatment temperatures between 600 – 900°C.

Lenarduzzi et al[7] suggest that the oxide growth is epitaxial as seen from the orientation between the oxide grains and underlying titanium grains using EBSD. They claim that pole figures obtained through EBSD shows the tendency for epitaxial growth of the oxide layer. This implies that, oxide grains will have the same orientation as the 'parent' titanium grain in which it has grown. They also suggest that the titanium oxide detected using x-ray diffraction is in the rutile and anatase form.

Zhang et al[3] report that XRD analysis revealed a sub-oxide layer below the TiO_2 layer that could consist of any of the following oxygen starved titanium oxides and combinations thereof: TiO, Ti_2O_3, Ti_4O_7 while the metal directly below this layer although still titanium metal could be in the oxygen rich titanium or the titanium compound phase.

Below the oxide layer a region will exist in the titanium metal that is oxygen enriched, but has a concentration below that required for titanium oxide formation. At a macroscopic level an oxide/metal interface exists between the oxide layer and the underlying metal and will forthwith be referred to as the interface.

2.2.3.1.2 Oxide layer quality and adherence

The adherence of the oxide layer to the metal is crucial as the oxide layer acts as the oxygen reservoir for the subsequent boost diffusion step. Delamination of the oxide

layer is caused by one of two factors. The first is the different thermal coefficients of expansion for the oxide layer and the alloy; this difference causes residual stresses that result in decohesion during cooling after step 1[7]. These stresses increase with oxide layer thickness and delamination of the oxide layer would therefore occur as a result of cooling after the oxidation step if the residual stresses are large enough. Delamination for thin oxide layers is not expected as adherent thin oxide layers after cooling have been reported[3,4,6].

The second reason for delamination of the oxide layer is the high Pilling-Bedworth ratio for titanium which is 1,95[34]. The ratio is determined by the comparison of the molar volume in the oxide layer to the molar volume in the metal[35]. When a metal has a ratio higher than 1 the volume of the formed oxide layer is larger than the volume of metal and this difference in volume at the interface causes tensile stresses in the metal and compressive stresses in the oxide layer. These compressive stresses cause delamination of the oxide layer from the metal. The adherence of the oxide to the metal, therefore, decreases as oxide layer thickness increases. The delamination of thick oxide layers is therefore unavoidable due to the high Pilling-Bedworth ratio of titanium[3,4]. If cooling was eliminated between step 1 and 2 of an OBDH treatment delamination could, therefore, still occur for thick oxide layers due to the compressive stresses in the oxide layer induced by the large volume change.

Dong et al[4] found that adherence of the oxide layer is maintained while maximum oxide layer thickness is achieved through an oxidation treatment step conducted at a temperature of 850^{o}C for a treatment time of 30 minutes or less. While similarly, Zhang et al[3] report the formation of a compact, relatively adherent oxide layer for treatment times of 40 minutes and shorter at 850^{o}C. For longer periods and higher temperature oxidation treatments, adherence decreased.

2.2.3.1.3 Diffusion hardening during the oxidation step

Oxygen atoms can diffuse through the TiO_2 layer; and in fact the diffusivity of oxygen in TiO_2 is 50 times higher than in titanium metal implying that the rate of diffusion movement is determined by the movement of oxygen in the metal under the oxide layer[4]. The hardening that occurs below the interface is directly related to the oxygen

concentration. The oxygen atoms diffuse into octahedral sites in the lattice causing lattice distortion, increasing dislocation build up which in turn increases metal strength and hardness. The diffusion hardening caused during the oxidation step therefore decreases with the oxygen concentration away to the interface.

Diffusion hardening during the oxidation step, with optimum oxide layer thickness and adherence, has been reported to depths of 50 µm for an oxidation treatment at 850^{o}C for 20 minutes[3]. Dong et al[4] reported an increase in hardness 75 µm from the interface for an oxidation treatment at 850^{o}C for 30 minutes.

2.2.3.2 Step 2: Boost diffusion

After the oxidation step an oxidised specimen is cooled and re-heated to temperatures above 600^{o}C in an oxygen free environment for extended periods of time.

2.2.3.2.1 Boost diffusion treatment conditions

Dong et al[4] found that the boost diffusion step could be conducted at temperatures between 700 – 900^{o}C. The best results however were obtained in their previous research, when the boost diffusion step was done at 850^{o}C. For temperatures below this longer treatments were needed, while at higher temperatures the remaining oxide layer would have poor adhesion to the metal. They did a range of treatments at 850^{o}C for 15 – 30 hours. The best combination of temperature and time was found to be at 850^{o}C for 20 hours. They found that the oxide layer had completely dissociated and that specimens had a bright metallic lustre after the boost diffusion step which was conducted under vacuum conditions of 1 x 10^{-4}Torr. Zhang et al[3] state that it is the high vacuum that is crucial for the dissociation of oxygen out of the oxide layer at the interface for boost diffusion to occur. The suggested vacuum is above 10^{-6}Torr. In contrast to the statement that high vacuum for boost diffusion to occur, Camagu[36] found that similar boost diffusion hardening can be achieved in titanium alloys that are diffused under argon conditions. These results indicate that low vacuum in not crucial for boost diffusion to occur.

2.2.3.2.2 Boost diffusion movement of oxygen

The boost diffusion step is conducted in an oxygen free environment; therefore, the only oxygen available for boost diffusion movement during this step is that in the TiO_2 layer (oxygen reservoir). A high oxygen potential will exist at the interface as long as the oxide layer exists[4]. Oxygen dissociates out of the TiO_2 and moves across the interface into the metal and this dissociation actively decreases the thickness of the oxide layer and causes the movement of the interface towards the surface of the metal. This is the reverse process of oxide layer growth that occurs during step 1[5]. For this reason surface adherence of the oxide layer is absolutely crucial to enable unhindered oxygen diffusion movement that causes boost diffusion hardening during the step 2.

The oxide layer is reported to disappear completely after very long treatment times under high vacuum. During the boost diffusion step the mass balance of oxygen that is boost diffused into the metal is equal to the oxygen decomposed out of the oxide layer[5]. X-ray diffraction (XRD) analysis, performed by Dong et al[4], showed rutile peaks after the oxidation step and the diminished rutile peak after the boost diffusion step. This illustrates that the rutile formed during the oxidation step almost completely dissociates during the boost diffusion step done under vacuum. They also reported α titanium peak broadening from the oxidation to the boost diffusion step illustrating the increase in dissolve oxygen in the alloy lattice.

Oxygen is a known α phase stabilizer so as the oxygen concentration decreases away from the surface through the substrate the presence of β grains should increase until the normalised α+β microstructure is reached. Dong et al[4] reported lower occurrence of β grains in the diffusion hardened zone. The suggestion is that in these regions with very high oxygen content, the inter-granular β grains are transformed into stable α grains.

Zhang et al[3] reported the presence of cracks and pores in a sub-oxide region during the dissociation process after 2, 5, 7, 8 and 10 hours of boost diffusion. The presence of these defects could be a result of the microstructural defects in the oxide or as a result of increased stresses due to high solid solution oxygen concentrations. They

suggest that after adequate time (20 hours) at temperature during the boost diffusion step annealing should occur which would reduce the amount of microstructural defects.

2.2.3.2.3 Influence of oxide layer thickness and adherence during boost diffusion

As discussed in section 2.2.3.1.2 in this chapter, two contributing factors exist that cause the delamination of the oxide layer. As the oxide layer serves as the oxygen reservoir for the step 2, delamination at the interface limits the boost diffusion hardening that can be achieved during this step. If the oxide layer formed during step 1 is not thick enough, the boost diffusion hardening during step 2 is also limited. This is seen clearly in the following diagram that compares the boost diffusion hardness (20 hours at 850^{o}C) achieved after three oxidation treatments of varying treatment times at 850^{o}C. The specimen oxidised for 30 minutes shows the highest increase in boost diffusion hardening, followed by the specimen oxidised for 15 minutes and finally the lowest increase in hardness is seen for the specimen oxidised for 45 minutes[4]. All three specimens were cooled after step 1, during which delamination of the oxide layer for the specimen oxidised for 45 minutes could have occurred, resulting in lower boost diffusion hardening.

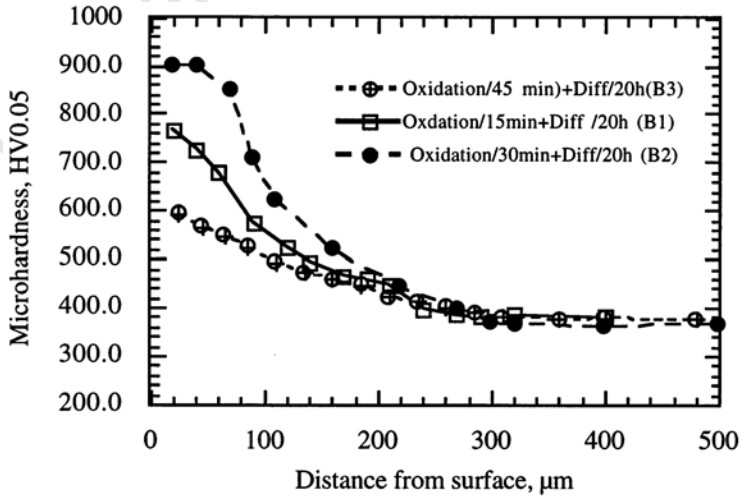

Figure 3: The influence of oxide layer thickness and adherence during the boost diffusion step[4].

2.2.3.3 The suggested boost diffusion mechanism

The equations of two reactions that could be responsible for the dissociation of the oxide layer, during step 2, are given by Dong et al[4]:

TiO_2 (solid) = Ti (solid) + O_2 (gas) (1)

TiO_2 (solid) + Ti (solid) = 2O (dissolved in titanium) (2)

The first reaction would occur at the oxide surface while the second at the oxide metal interface. During both these reactions oxygen would dissociate out of the oxide. The partial pressure of TiO_2 at 850^{o}C, is known to be as low as 3.29 x 10^{-28}Torr while the partial pressure in the treatment chamber and consequently at the oxide surface is 1 x 10^{-3}Torr. Freed oxygen (dissociated out of the oxide) will diffuse into the metal due to the very low partial pressure and not lost to the vacuum treatment environment.

The argument is that if the first reaction occurred, the hardening during the boost diffusion step would not be any deeper than the diffusion hardening during the oxidation step because the oxygen liberated at the surface would be extracted by the high vacuum. The boost diffusion hardening depth is much greater which entails that the second reaction (2) occurs during step 2. A high oxygen potential will exist at the interface as long as the oxide layer is present and diffusion movement into the metal will occur due to the steep oxygen concentration gradient.

Zhang et al [3] examined SEM images of pre-oxidised specimens after 2, 5, 7, 8 and 10 hours of boost diffusion and reported the changes in the near surface region as proof that the oxide layer had dissociated. The images showed that an intermediate oxide layer formed during interaction between the TiO_2 layer and the metal substrate. Oxygen concentration measurements in the oxide layer showed sub-TiO_2 stoichiometry concentrations and that the oxygen concentration in the oxide layer was lowest at the interface. XRD analysis showed the presence of oxygen deficient oxides TiO, Ti_2O_3 and Ti_4O_7 in the intermediate layer region. During oxide layer dissociation (step 2) the oxide layer stoichiometry is given as: Ti_aO_b and not TiO_x where $b > a > b/2$.

Reactions between the titanium metal and TiO_2 could result in the release of oxygen to form sub-oxides during the following reaction:

TiO_2 (solid) +Ti (solid) = Ti_aO_b + x.O (dissolved in titanium and oxide) (3)

Oxygen formed during this reaction at the interface is now free to dissolve into the metal substrate; this oxygen is dissolved into the metal and does not result in weight loss.

Zhang et al[3] suggest that the driving force for the continuous diffusion movement of oxygen into the metal substrate is the concentration gradient of dissolved oxygen that already exists in the substrate. The oxygen concentration in metal below the oxide was expected to be that of the maximum oxygen concentration before stoichiometry is reached for TiO_2 formation. However, the expected concentration was not found using XRD analysis. In fact, a discontinuity in oxygen concentration in the metal at the interface was reported. The explanation given for this concentration discontinuity is the insufficient dissociation rate of the oxide. The rate at which oxygen dissociates out of the oxide is not high enough to free up enough oxygen to fill all the positions emptied during the diffusion movement in the metal at the interface which occurs at a higher rate. This difference between the dissociation and diffusion movement rates results in the oxygen concentration discontinuity.

If the dissociation rate of oxygen out of TiO_2 at the interface is adequately high and enough oxygen is released, the concentration of oxygen in the sub-oxide at the interface should equal that of the oxygen concentration of the metal below the sub-oxide at the interface. This was however not seen in the X-ray spectroscopy (EDX) results.

2.2.4 Nitrogen diffusion

Titanium is known to react with nitrogen at elevated temperature. When the oxidising medium utilised during step 1 contains both nitrogen and oxygen the titanium metal will, therefore, react with elements from both gasses. Both nitrogen and oxygen atoms diffuse into interstitial positions in the crystal lattice. Once seated in interstitial

positions nitrogen atoms are slower in moving to a deeper position further away from the surface. In fact, deeper diffusion movement of nitrogen atoms in titanium metal is not really believed to occur[7]. As there are only a finite amount of interstitial positions available for diffusion movement, the presence of nitrogen is suggested to retard the diffusion movement of oxygen. This limits the final boost diffusion hardening that would have been achieved had the oxidation step been conducted in a pure oxygen environment. The reported build up of nitrogen occurs at the oxide-metal interface. The suggestion is that nitrogen does not practically diffuse in the metal resulting in the build up of nitrogen[6].

Lenarduzzi et al[7] conducted oxidation treatments in O_2 + Ar gas environments as well as O_2 + N_2 environments. Mass gains measured after treatments during which nitrogen was present, were lower than for treatments in which nitrogen was absent. They explain the reason for nitrogen build up at the interface as follows. The atomic structure for rutile contains large enough sites for N_2 to diffuse through the oxide layer. The nitrogen then dissociates at the interface. As nitrogen does not really practically diffuse deeper into the metal it now stays in interstitial positions at the interface blocking diffusion movement of oxygen. The following figure illustrates the build-up of nitrogen at the oxide metal interface.

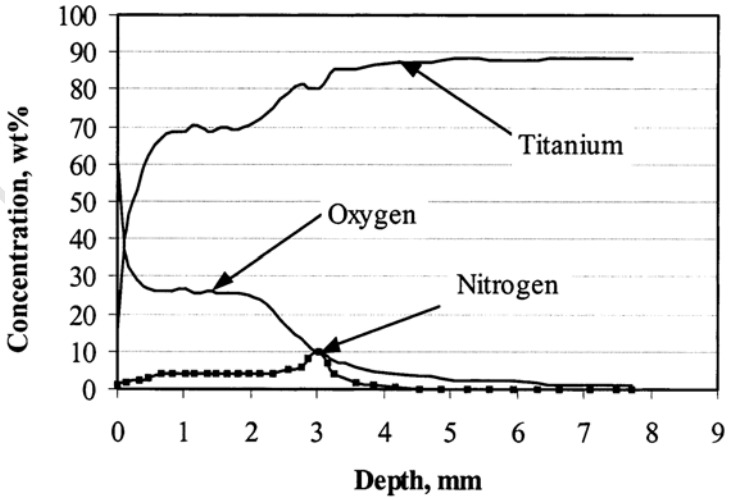

Figure 4: Composition profiles illustrating the nitrogen build up at the interface of a Ti-6Al-4V specimen oxidised in air[4].

3 EXPERIMENTAL PROCEDURE

3.1 Specimen preparation

3.1.1 Surface treatment specimens

Ti-6Al-4V specimens used for surface hardening treatments were sectioned into 5mm thick disks from wrought and cold rolled annealed 16 mm diameter round bar of high purity with an IMPTECH EUROPE abrasive cutter using a silicon cutting blade (TRE 40). The alloying composition of the Ti-6Al-4V alloy utilised can be seen in Table 1 in section 2.1.5. This specific type of blade minimises deformation during cutting of titanium alloys. These sectioned disks were set in clear acrylic resin using a Struers LaboPress-3. A force of 20 kN was used for resin compression and 6 minutes was allowed for heating and another 6 minutes for cooling[37].

A Struers RotoPol – 22 automatic polisher with a Struers RotoForce-4 polisher head was used for grinding and polishing of specimens. Grinding paper of 220, 500, 800 grit and followed with 1200 grit was used to grind both faces of the flat disk, with water as lubricant. The rotational speed used was 300 rpm with both the specimen holder and grinding medium rotating in the same direction. A downward force of 30 N was applied to specimens. Specimens were removed from the resin and both sides of the specimen ground on 4000 grit paper by hand. Detergent was used to degrease specimens after which they were rinsed in copious amounts of fast running tap water followed by a distilled water rinse and forced air dried.

3.1.2 Hardness testing and microscopy specimen preparation

Heat treated specimens were sectioned, normal to the flat surface of the disk using a BUEHLER IsoMet LOW SPEED SAW with a diamond imbedded cut-off wheel. This slow cutting method was used to ensure that no heat was generated during cutting, which could alter the microstructure of heat treated specimens or unnecessarily disrupt the surface layer.

The half-moon shaped specimens were placed with the newly sectioned surface down and set in resin. Grinding and polishing was done using a Struers RotoPol – 22 automatic polisher with a Struers RotoForce-4 polishing head and the grinding polishing procedure followed as given in the table below:

Polishing medium	**Lubricant**	**Force (N)**	**Time**	**Rotational speed (RPM)**	**Rotational direction (polishing head VS polishing pad)**
500 grit grinding paper	Water	30	until planer	300	Same direction
Silk cloth	9µm colloidal silica	30	10 min	150	Contra
MD NAP	Attack solution	30	10 min	150	Contra
MD NAP	Water	30	10 min	150	Contra

Table 3: Polishing method used to prepare heat treated specimens for microscopy and hardness testing.

The attack solution[38] used during sample polishing was made up of 50 mL of colloidal silica solution and 10 mL hydrogen peroxide. The attack solution is used to remove metal deformed through scratching during the grinding and polishing steps. The removal of deformed metal using the attack solution ensures good pattern quality during electron microscopy. Specimens were removed from the sample holder and degreased using detergent after which they were rinsed in copious amounts of tap water to remove any detergent and then rinsed in distilled water and finally forced air dried.

3.1.3 Scanning electron microscope specimens

Specimens prepared according to the procedure given in Table 3 were removed from the resin mounting and fixed to an aluminium stub using LEIT-C Conductive Carbon Cement. This cement ensures specimens do not become charged during SEM imaging.

3.2 Hardness testing

3.2.1 Microhardness

Guleryuz et al[2] reported a hardness increase only up to 20 µm from the surface for a specimen oxidised at 600°C for 60 hours. They measured the Vickers hardness using 10 gram force as close as 1 µm from the surface. Zhang et al[3] used loads of 25 and 50 gram force to measure hardening during the OBDH process as close as 10 µm from the surface. Dong et al[4] used microhardness profiles, measured at a distance of 20 µm from the surface using 50 gram force, to compare hardening results after step 1 conducted for varying treatment times at 850°C, as well as for step 2 conducted for different treatment times at 850°C. Hardening was measured up to 75 µm from the surface after step 1 and 300 µm after step 2.

A MATSUSAWA MXT-CX7 Optical Microhardness Tester was used to conduct hardness measurements on heat treated specimens to determine and compare the hardening that occurred during different treatments. A static load of 50 gram force was used to indent test material with a pyramid shaped diamond indenter. This load was used as the indents were big enough to measure accurately, but, still small enough to get within 20 µm of the interface. The hardness of the bulk was known to be 350 HV and this value did not change during heat treatments.

3.2.2 Nanohardness

Indentation was done on a CSM NHTX S/N: 25-0024 instrument applying a load of 5 gram force (50 mN). Access to the instrument was limited and only a few indents could be made for each specimen. Nanoindents were programmed to be made as close as possible to the interface; in some cases indents were made as close as 3 µm. Nanohardness results were used to determine and compare the hardening that occurred close to the interface during different heat treatments. The distance programmed between indents was selected to ensure that indents did not overlap and can be seen in the figure below.

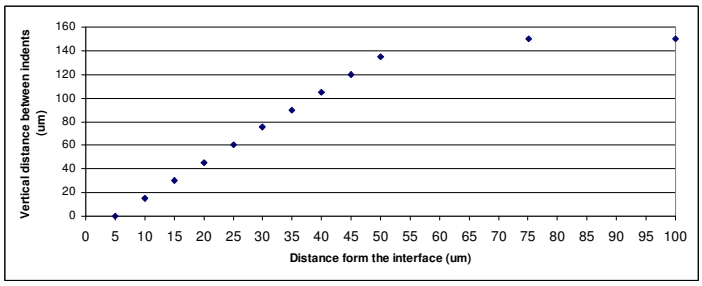

Figure 5: Programmed positions illustrating the distances between nanoindents.

3.3 Optical light microscopy

A Nikon optical light microscope fitted with a Leica EC3 camera attached to a computer using the LAZ ES Leica application suite data acquisition programme was used. Heat treated specimens were sectioned and polished to a mirror finish according to the method discussed in section 3.1.2. To determine the interface integrity, quality and thickness of the oxide layers formed during oxidation experiments, images of this region were recorded and these images compared in chapter 4.

3.4 Tube furnace vacuum system

3.4.1 Tube furnace low vacuum system

Initially only a BOC Edwards two stage rotary pump was used to provide vacuum conditions in which the boost diffusion step could be conducted in the tube furnace. The highest attainable vacuum using this system was 2 x 10^{-2}Torr. The following schematic diagram shows the initial set up for the quartz tube furnace.

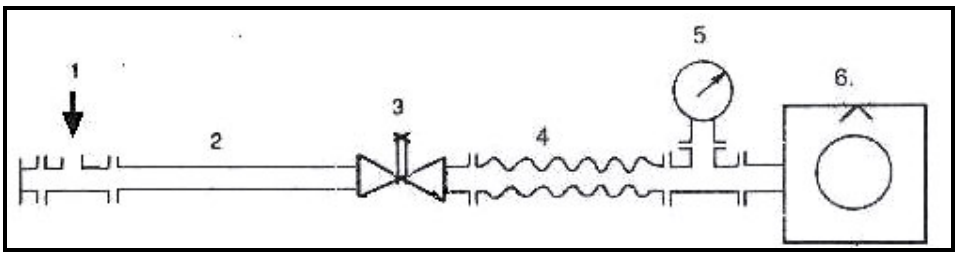

Figure 6: Schematic diagram of the low vacuum tube furnace system.

Where:

1. Controlled flow air inlet
2. Vacuum chamber
3. Crack valve
4. Soft vacuum tubing
5. Backing vacuum gauge
6. Rotary backing pump

3.4.2 Modified vacuum system

The setup was modified to increase the vacuum level as the boost diffusion step had to be conducted under high vacuum conditions. A turbomolecular pump was introduced into the system to increase the vacuum to 10^{-4}Torr. The following diagram shows the final tube furnace vacuum system setup.

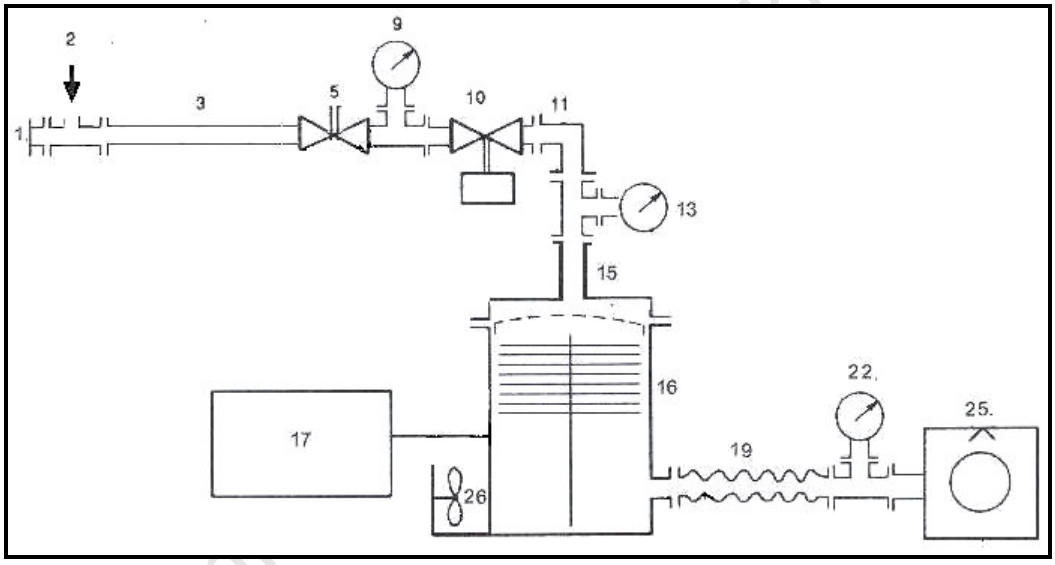

Figure 7: Schematic diagram of the modified vacuum system for the tube furnace to achieve high vacuum.

Where

1. End cap.
2. Controlled gas flow inlet
3. Vacuum chamber (Quartz tube)
5. Crack valve
9. Low vacuum diaphragm gauge
10. Cut off valve (Speedi valve)
11. 90 degree elbow
13. High vacuum Penning gauge
15. ø 95 mm to ø 30 mm reducer
16. Turbomolecular pump
17. Turbomolecular pump controller
19. Soft vacuum tubing
22. Backing pressure Pirani gauge
25. Rotary backing pump

26. Air cooling system

In order to modify the existing system a stand was designed to locate the turbomolecular pump on. The stand, as well as some vacuum fittings, were manufactured in the mechanical engineering workshop at the University of Cape Town. The machine drawings for these components are presented in Appendix A.

3.5 Initial surface hardening experiments

3.5.1 Tube furnace

Most heat treatments discussed in this chapter were conducted in the ELITE tube furnace. The only exceptions were the preliminary boost diffusion experiments (3.5.3) which were conducted in an upright vacuum furnace and the box furnace oxidation treatment (3.5.4.1). The furnace heating and cooling rate used was 5^{o}C/minute. This rate insured that no thermal shock was experienced by the quartz tube. Two specimens were subjected to each treatment. Specimens were positioned in the hot spot of the furnace at the centre of the tube and the system sealed. A rotary backing pump removed the air by pumping the treatment chamber down to a vacuum of 10^{-2}Torr. During oxidation experiments the pump was switched off and the oxidising medium purged into the system until atmospheric pressure was reached. This ensured that oxidation medium was not contaminated. For vacuum boost diffusion experiments the backing pump remained on and the turbomolecular pump was utilised to maintain high vacuum of 10^{-4}Torr, or for argon diffusion the backing pump was switched off and argon purged through the chamber continuously. Both, vacuum and argon diffusion result in boost diffusion hardening of the Ti-6Al-4V alloy, as discussed in section 2.2.3.2.1. Boost diffusion steps were conducted to determine which of the two treatment environments resulted in higher boost diffusion hardening.

3.5.2 Preliminary oxidation experiments

Initial oxidation heat treatments were conducted to determine the response of the alloy for different oxidation experiments. Treatments with varying times and temperature

parameters, as given in the table below, were conducted. Pure oxygen of 99, 95 % purity was used as an oxidising medium during all four treatments. Ground and degreased specimens were oxidised in the tube furnace according to the parameters given in Table 4. The oxygen was purged through the chamber continuously at a positive pressure of 60 Torr during the oxidation step.

Treatment	Temperature (^{o}C)	Dwell time at temperature	Oxidation medium	Type of gas flow
650/0.75	650	45 minutes	Oxygen	Continuous
650/3	650	3 hours	Oxygen	Continuous
850/6	850	6 hours	Oxygen	Continuous
850/0.5	850	30 minutes	Oxygen	Continuous

Table 4: Preliminary oxidation experiment treatment parameters.

3.5.2.1 Oxide scaling due to fast cooling

Specimens were left to furnace cool to room temperature to ensure that all specimens experienced the same cooling rate (5^{o}C/min). Delamination of the oxide layer would therefore be due to cooling as a result of oxide thickness and not as a result of cooling rate.

3.5.3 Preliminary boost diffusion experiments

From experiments previously conducted at the centre[36] and reviewed OBDH literature[4], the optimum combination of time and temperature for the boost diffusion step was 20 hours at 850^{o}C in one of two oxygen free environments: argon or high vacuum. These experiments were conducted in the upright vacuum furnace of which the heating and cooling rate was 5^{o}C/minute. Specimens were furnace cooled to room temperature after the boost diffusion treatments. Pre-oxidised specimens from the preliminary oxidation experiments were suspended in the upright furnace and heat treated according to the boost diffusion treatment parameters in the table below:

Treatment	Treatment temp (^{o}C)	Treatment time (hours)	Environment
650/0.75/Ar	850	20	Argon
650/3/Ar	850	20	Argon
850/5/Ar	850	20	Argon
850/0.5/Ar	850	20	Argon
850/0.5/Vac	850	20	Vacuum

Table 5: Preliminary boost diffusion experiment parameters.

3.5.3.1 Argon environment boost diffusion

For treatments which required an argon environment for the boost diffusion step the following procedure was followed: the chamber pressure was lowered to a vacuum of 10^{-4}Torr and the temperature raised. When temperature was reached the pump system was switched off and argon purged into the chamber until atmospheric pressure was reached.

3.5.3.2 High vacuum boost diffusion

For the boost diffusion treatment which required a high vacuum environment for step 2, the following procedure was followed. The furnace temperature was raised and vacuum of 10^{-4}Torr maintained for the duration of the boost diffusion step. These experiments were conducted in the upright furnace as the tube furnace could not achieve the required high vacuum. Experiment were conducted in the tube furnace as soon as the tube furnace system was modified, as noted in section 3.4.2, to achieve vacuum of 10^{-4}Torr .

3.5.4 Oxidation medium experiments

Oxide layer quality and adhesion to the metal remained a problem even though cooling rate had been eliminated as a contributing factor. The oxide appearance of the oxide layer on the top and bottom surfaces of heat treated specimens were not consistent; some oxide layers had a mottled appearance and flow patterns. Four different oxidation treatments were conducted to determine whether surface adhesion and oxide quality could be improved by changing the oxidising medium and the type

of gas flow. Specimens were prepared for each oxidation treatment according to the method discussed in 3.1.1. The composition of the medical air use in these experiments contained 21 % oxygen and 79 % nitrogen. Three of the four treatments were done in the tube furnace (section 3.5.1) while the fourth was conducted in the box furnace. The different treatment parameters of these four oxidation treatments are summarised in Table 6 below and explained in more detail in sections 4.3.3.1 – 4.3.3.3.

Treatment	**Treatment Temp (^oC)**	**Treatment time (min)**	**Oxidation Medium**	**Gas flow**	**Cooling Rate (^oC/min)**
Box furnace	850	30	Air	Stagnant	5
Pulsed O_2	850	30	Oxygen	3 x 1 min pulses	5
Pulsed MA	850	30	Medical air	3 x 1 min pulses	5
CF MA	850	30	Medical air	Continuous flow	5

Table 6: Oxidation medium experiment treatment parameters.

3.5.4.1 Box furnace oxidation experiment

Specimens were inserted into a box furnace and oxidised in natural air at 850^{o}C for 30 minutes and furnace cooled to room temperature. The box furnace heating and cooling rate was set to be the same as that of the tube furnace (5^{o}C/min) to ensure consistency.

3.5.4.2 Pulsed gas flow oxidation experiments

Treatments Pulsed O_2 and Pulsed MA were conducted as follows: To eradicate the flow patterns in the oxide layer the oxidising medium was pulsed through the tube for the first, tenth and twentieth minute of the oxidation step and the gas flow turned off. After 30 minutes, the furnace temperature was dropped to room temperature and the specimens removed. The following diagram illustrates the pulsed gas flow procedure during an oxidation treatment.

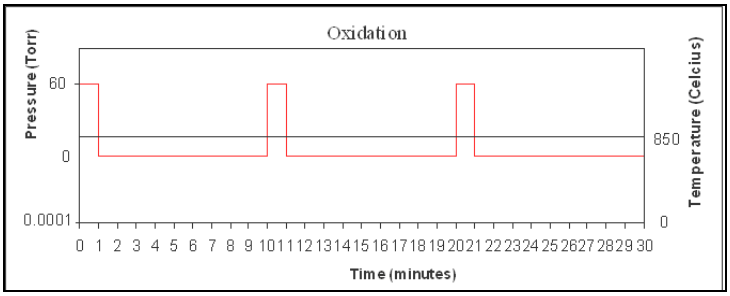

Figure 8: Illustration of oxidation treatments conducted under pulsed gas flow conditions.

3.5.4.3 Continuous gas flow oxidation experiment

Specimens were inserted into the tube furnace and a vacuum of 10^{-2}Torr created where after medical air was purged into the system until atmospheric pressure was reached. As soon as temperature was reached medical air was purged into the furnace continuously for 30 minutes. The gas flow was turned off and the temperature dropped to room temperature. The following diagram depicts the process that was followed during treatment CF MA.

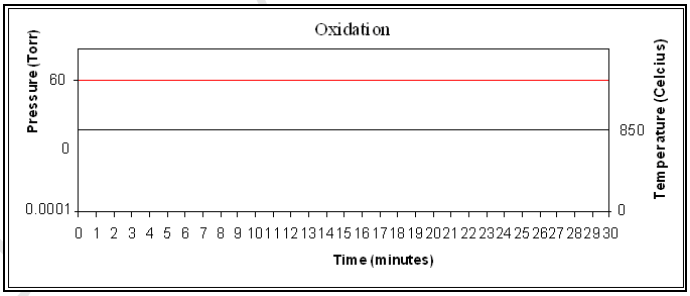

Figure 9: Illustration of continuous gas flow oxidation conditions.

3.6 OBDH experiments

To maintain oxide layer adherence as far as possible during these experiments, specimens were left in the furnace between the oxidation and boost diffusion treatment steps that included cooling, thus eliminating handling of oxidised specimens which could cause the oxide layer to separate from the specimen. All the OBDH experiments discussed in this section (3.6) were conducted in the high vacuum tube

furnace system. During these experiments the boost diffusion environment was always maintained until the furnace temperature had dropped to 200°C during cooling after the boost diffusion step. It was not necessary to maintain the diffusion environment below this temperature as the diffusion movement of oxygen is negligible at such low temperatures.

3.6.1 Thermal profile design

Oxide layer separation could occur as a result of thickness during cooling after step 1 of an OBDH treatment. Therefore, in order to try and optimise boost diffusion hardening a continuous isothermal treatment was introduced during which no cooling occurred between step1 and step 2. By comparing the boost diffusion hardening achieved through a continuous isothermal treatment to that of a treatment which included cooling, it was possible to determine whether boost diffusion hardening could be optimised by eliminating cooling while keeping all other treatment parameters identical. This isothermal profile treatment also shortened the total time from start to finish of the OBDH treatment as the cooling and reheating after step 1 was now eliminated.

3.6.1.1 Continuous isothermal OBDH treatments

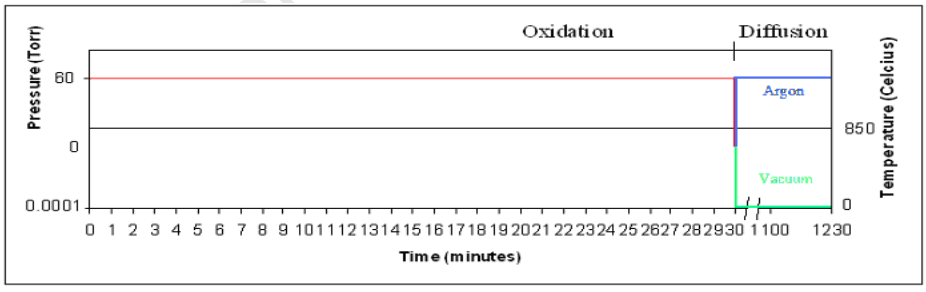

Figure 10: Illustration of a continuous isothermal OBDH treatment with continuous flow of the oxidation medium during step 1.

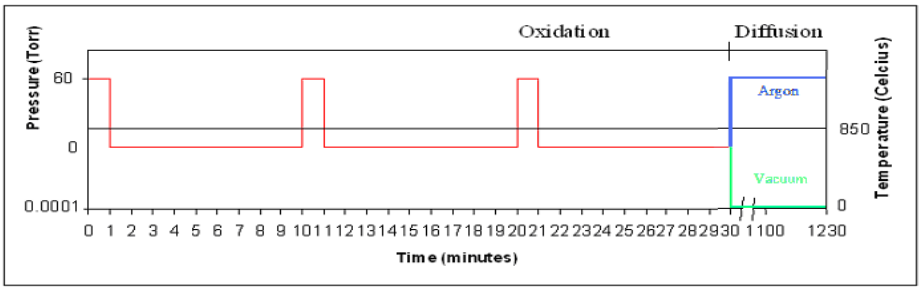

Figure 11: Illustration of a continuous isothermal OBDH treatment with Pulsed oxidation medium gas flow during step 1.

Figure 11 and Figure 12 illustrate the thermal profile and that the boost diffusion step in these treatments can be conducted in either an argon or high vacuum environment. During the continuous isothermal treatments the boost diffusion step was conducted immediately after the oxidation step. The tube furnace setup enabled that the oxidising medium could be removed and the diffusion environment created instantly. Vacuum of 10^{-4}Torr was maintained for vacuum boost diffusion steps, while argon was continuously purged at a pressure of 60 Torr for argon diffusion steps.

3.6.1.2 Interrupted thermal OBDH treatments

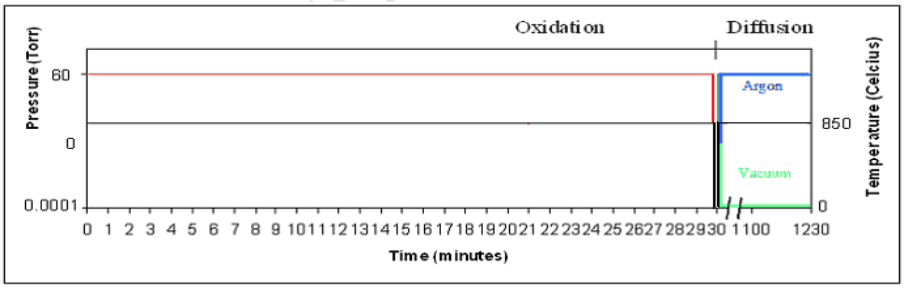

Figure 12: Illustration of an interrupted thermal OBDH treatment with continuous oxidation medium flow during step 1.

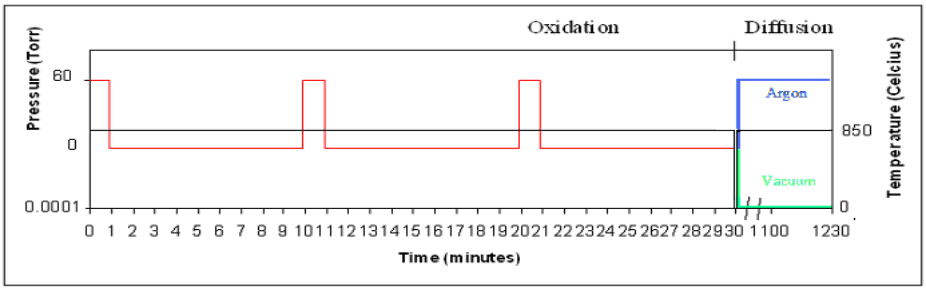

Figure 13: Illustration of an interrupted thermal OBDH treatment with pulsed oxidation medium gas flow during step 1.

The illustration in Figure 12 and Figure 13 depicts the interrupted thermal profile for conventional two step OBDH treatments which include cooling after the oxidation step. These figures illustrate that the subsequent step 2, after cooling, can be conducted in either an argon or high vacuum environment.

3.6.2 Cyclic isothermal OBDH treatments

A novel method was designed in which the total oxidation and boost diffusion treatment times were broken into three shorter cycles. The first 10 minute cyclic oxidation step would be followed by a short cyclic boost diffusion step of 6.5 hours. These cycles would be repeated until the 30 minutes of oxidation and 19.5 hours of boost diffusion treatment time had been reached with no cooling between steps.

The hypothesis was that during these shorter oxidation treatments of ten minutes, thin adherent titanium oxide layers would be formed, and that during the subsequent boost diffusion treatment most of the oxygen from this thin oxygen reservoir would diffuse into the metal. This movement would almost completely dissolve the thin oxide layer. This would then immediately be followed by a second oxidation and boost diffusion treatment (isothermal profile). As no delamination of the oxide layer due to cooling or thickness was assumed to occur during these cyclic treatments the boost diffusion hardening was expected to be better than for treatments in which a thicker oxide layer was formed and delamination could occur during cooling between treatment steps.

The boost diffusion hardening results for cyclic treatments were compared to that of the two step treatment with cooling as well as to those with no cooling between steps for which all other treatment parameters were identical.

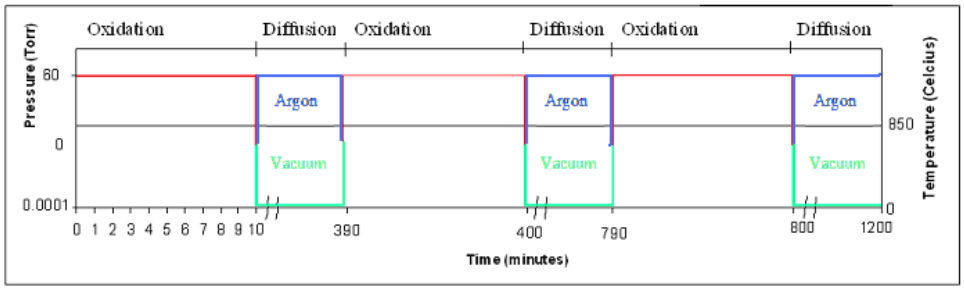

Figure 14: Illustration of cyclic isothermal OBDH treatments with continuous flow oxidation mediums during step 1.

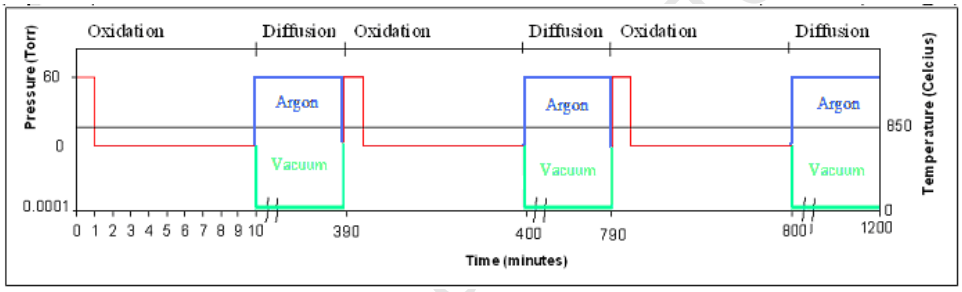

Figure 15 : Illustration of cyclic isothermal OBDH treatments with pulsed oxidation medium gas flow during step 1.

During the cyclic isothermal treatments, as illustrated in Figure 14 and Figure 15, shorter oxidation treatments were immediately followed by cyclic boost diffusion treatments until 30 minutes of oxidation and 19.5 hours of boost diffusion had been conducted. As illustrated in the images above, step 2 could be conducted under either a high vacuum or an argon environment.

3.6.3 Heat Treatment Matrix

The following matrix was designed so that the treatment parameters could be compared:

- two different oxidising mediums
- two different oxidation medium gas flow methods
- two different boost diffusion environments were also included

- two different thermal profiles
- cyclic treatments

Oxidation / Boost diffusion	Continuous O_2 flow	Continuous MA flow	Pulsed O_2	Pulsed MA
Continuous isothermal argon flow			Pulsed O_2/Ar	
Continuous isothermal vacuum			Pulsed O_2/Vac	
Cyclic isothermal vacuum	Cyclic/CF O_2/Vac		Cyclic/Pulsed O_2/Vac	Cyclic/Pulsed MA/Vac
Interrupted thermal argon flow			Pulsed O_2/cool/Ar	
Interrupted thermal vacuum	CF O_2/cool/Vac	CF MA/cool/Vac	Pulsed O_2/cool/Vac	Pulsed MA/cool/Vac

Table 7: Heat treatment matrix.

3.7 Microstructural Analysis

3.7.1 Scanning electron microscopy

Secondary electron and backscattered electron imaging (EBSD) was used to examine the metallografic structures in order to understand of the mechanism at work during the boost diffusion process. Imaging was conducted on oxidised as well as fully boost diffusion treated specimens prepared for microscopy according to the method given in section 3.1.3. These images were obtained in a LEO 1525 FEGSEM (Field Emission Gun Scanning Electron Microscope). The operating voltage used was between 15-20 kV: the lower voltage condition was selected to minimise the extent of charging on the titanium oxide layer. However, it was also important to adjust the microscope conditions to ensure reasonable pattern quality and thus a compromise was sometimes made within this voltage range. The step size used to acquire EBSD maps was varied depending on the size of the imaged area, as well as the grain size distribution within

the imaged area. An Oxford Inca System was used to generate EBSD orientations maps.

3.7.1.1 Oxidised specimens

The specimens that were analysed in this section were oxidised under pulsed oxygen conditions for 30 minutes at 850^{o}C. Both secondary electron images and EBSD orientation maps were used to gather information about grain size distribution and grain orientation of oxidised specimens. The regions of interest for microstructural analysis were those regions at the near surface of the specimens which included the oxide layer, the interface and the underlying titanium metal. Analysis was done on the oxide layer to determine the mechanism responsible for the formation and growth of the oxide layer. The underlying metal was also investigated to determine the grain size distribution in the underlying metal as well as the β grain distribution after the oxidation step.

3.7.1.2 Boost diffused specimens

The specimens that were analysed were specimens from treatment Cyclic/Pulsed O_2/Vac and treatment Pulsed O_2/cool/Vac from the heat treatment matrix. Again, both secondary electron images, and EBSD orientation maps were used to investigate the microstructural changes that occur during step 2 so that the boost diffusion mechanism could be better understood. The region of interest, therefore, included the oxide layer, interface and near interface titanium metal as very little was known about the microstructural changes that occurred in this region during the boost diffusion step. These SEM images were also used to determine the grain size in the underlying metal to determine the grain growth that occurs during step 2.

4 EXPERIMENTAL RESULTS AND DISCUSSION

4.1 Preliminary oxidation experiment

The hardening results in this section were obtained by making five indents using a microhardness indenter and a 50 gram force at distances of 20, 45, 70, 100, 130, 160, 200 and 300 µm from the interface. The average value for each distance increment was calculated and error bars plotted to show the highest and lowest hardness values about the average.

4.1.1 Diffusion hardening during the oxidation step

The following section characterises specimens that have undergone the oxidation treatment step of the OBDH treatment in an oxygen rich environment, during which diffusion movement of oxygen into the metal occurs. This diffusion movement causes simultaneous TiO_2 layer formation when the dissolved oxygen content reaches stoichiometry and increased hardness of the metal below the oxide layer and is hence referred to as diffusion hardening. The purpose of the preliminary study is to test the response of the titanium alloy during different oxidation treatments.

The diffusion hardening increases with dissolved oxygen concentration, therefore, hardness measurements of this diffusion hardened zone are indicative of the amount of oxygen that dissolved into the metal during the oxidation step. The hardness of oxidised specimens was measured to determine which oxidation treatment allowed for the highest rate of oxygen diffusion movement. Optical light microscopy was utilised to examine the oxide layers formed during the oxidation treatments to determine the oxide layer thickness and integrity of the interface.

The preliminary oxidation experiments showed that the highest diffusion hardening as well as the deepest hardening depth of 140 µm below the interface was achieved during treatment 850/6. Treatment 850/0.5 achieved slightly lower increase in hardness and shallower penetration depth (100 µm). Treatments 650/0.75 and 650/3 both resulted in low diffusion hardening as well as very shallow penetration depths (70 µm). The profiles can be seen in Figure 16 below.

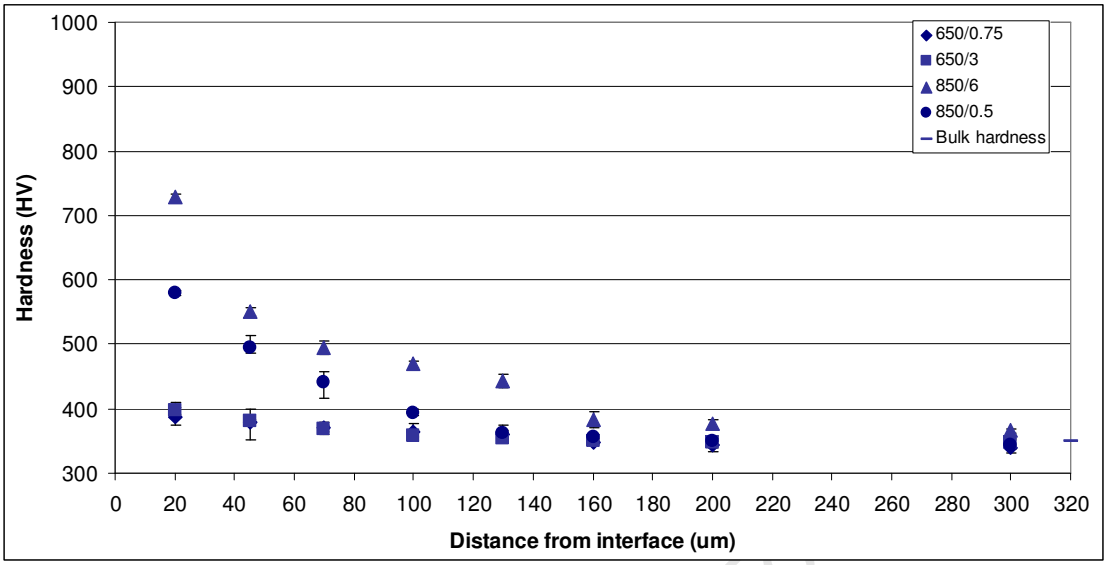

Figure 16: Comparative microhardness profiles for the preliminary oxidation experiment treatments.

4.1.2 Surface integrity after oxidation

Oxide layer formation occurs through the transformation of oxygen enriched titanium metal into rutile[3,4] TiO_2 and continues in the same direction as the oxygen diffusion movement into the metal. The diffusion movement rate is temperature controlled; therefore, higher treatment temperatures cause higher diffusion rates which will cause thick oxide layer growth in a short amount of time. At a certain oxide layer thickness stratification of the oxide layer will begin due to stresses induced by the large increase in volume causing a lamellar oxide layer which has poor adhesion to the underlying metal at the interface. At higher oxidation treatment temperatures this critical thickness is reached after a shorter amount of time.

4.1.2.1 Oxide adhesion as a function of cooling rate

Oxide layer adhesion was found to be very poor on oxidised specimens that were removed from the furnace at high temperatures as a result of the relative fast cooling rate that occurs after removal. The oxide layer and underlying diffusion hardened metal have different thermal expansion coefficients, therefore, during cooling two

different materials contract at different rates causing poor oxide layer adhesion to the metal at the interface. Under fast cooling conditions the dissimilar contraction rates would be more pronounced than under slow cooling conditions. This removal at high temperatures was conducted initially, where after it was decided to leave all samples to furnace cool. This ensured that all specimens experienced the same cooling rate.

Slow cooling was achieved through a furnace cooling rate of 5^{o}C/minute. Scaling and delamination of a thick oxide layer during cooling after step 1, is inevitable due to the high Pilling-Bedworth ratio[4], therefore, some delamination of the oxide layer was expected as a function of oxide layer thickness. However, by using the same cooling rate for all oxidised specimens, oxide layer adhesion as a function of cooling rate would be the same. Thus delamination due to oxide layer thickness for different oxidation treatments could be compared without being influenced by cooling rate.

4.1.2.2 Oxide layer appearance

The oxide layer formed during step 1 serves as the oxygen reservoir for the subsequent step 2, during which the oxygen moves out of the oxide across the interface and into the metal. The thickness of the oxide layer and the interface integrity, therefore, play crucial roles during the boost diffusion step.

The optical light microscope image in Figure 17 shows the oxide layer formed during treatment 850/6 to be as thick as 40 µm in some places with stratification within the layer clearly visible as well as delamination of the oxide layer at the interface illustrating that the treatment resulted in very poor interface integrity and a very thick lamellar oxide layer.

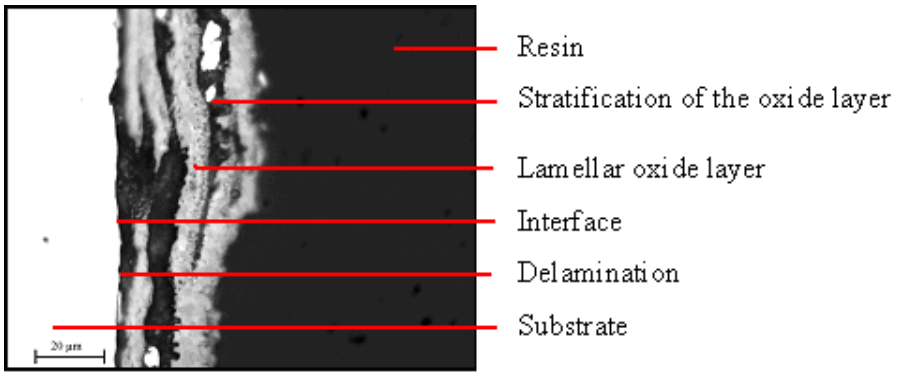

Figure 17: Delamination and stratification of the oxide layer formed during oxidation treatment 850/6.

The TiO_2 layer formed during treatment 850/0.5 in Figure 18, is in the order of 10 µm thick. The thickness of the layer is observed to be uniform with no delamination at the interface and no stratification within the layer. The treatment therefore resulted in an adherent oxide layer with acceptable thickness.

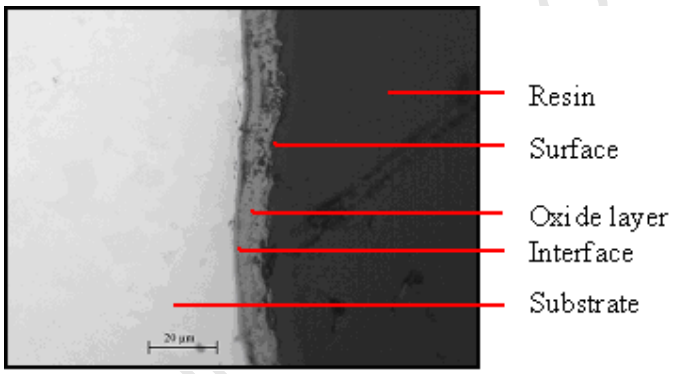

Figure 18: Adherent oxide layer formed during oxidation treatment 850/0.5.

The difference in appearance and thickness between the TiO_2 layers formed during the two treatments is ascribed to the fact that treatment 850/6 was kept at temperature for a much longer time than treatment 850/0.5 (6 hours vs. 30 minutes). At 850°C the rate of oxygen diffusion movement is high and during the long treatment time TiO_2 layer reaches critical thickness at which point stratification starts occurring within the oxide layer during cooling. Luo et al[5] suggest that during extended periods of oxidation, growing oxide layers reach a critical thickness after which exfoliation of

the oxide film occurs giving rise to a multi-layered (lamellar) oxide layer (Figure 17). For shorter periods this lamellar oxide growth does not occur as seen in Figure 18.

The oxide layer that was formed during oxidation treatment 650/0.75 is shown in Figure 19. The oxide layer is very thin with uniform thickness in the order of 2 µm. No delamination of the oxide layer at the interface or stratification is observed.

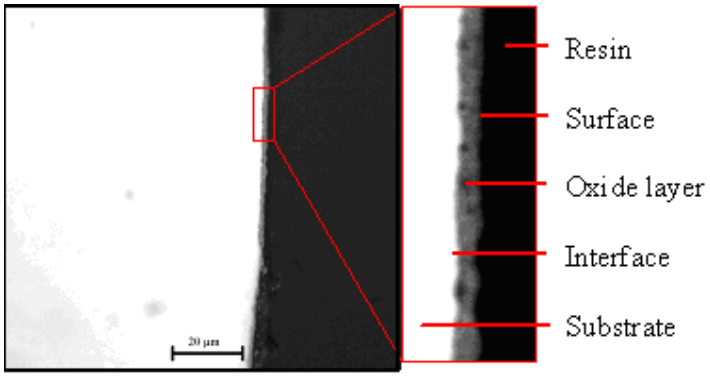

Figure 19: Thin adherent oxide layer with uniform thickness formed during oxidation treatment 650/0.75.

The oxide layer formed during oxidation treatment 650/3 has uniform thickness of 3 µm. Some separation between the layer and the underlying metal at the interface is observed.

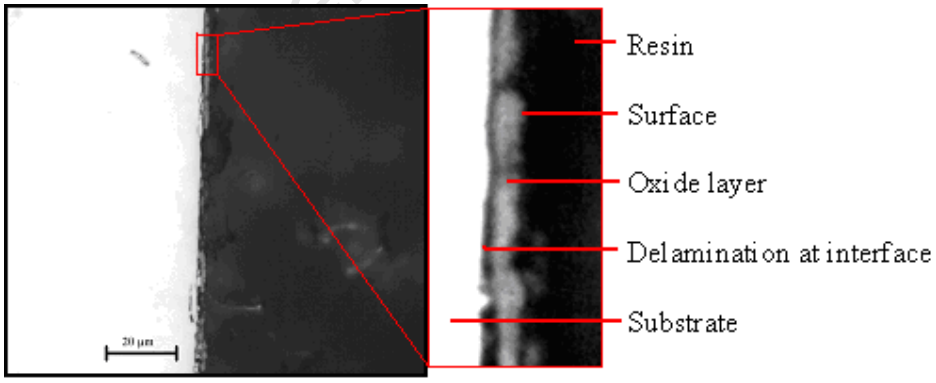

Figure 20: Oxide layer formed during oxidation treatment 650/3.

The difference in thickness for the oxide layers formed during the oxidation treatments at 650°C was very small: 2 µm thick after 45 minutes and 3 µm after 3

hours. The reason for the slight difference is due to the low rate of oxygen diffusion movement at low temperatures[4]. The 650/0.75 treatment was found to have good interface integrity compared to that of treatment 650/3 during which some delamination occurred lowering the interface integrity.

4.1.3 Oxygen diffusion as a function of treatment temperature

Zhang et al[3] report that the rate of oxygen accumulation is highest at a temperature range between 800°C and 900°C. They reported that the weight increase of a treated specimen after an oxidation treatment of 60 minutes at 800°C was 0.661 mg/cm^2 while the weight gain was 0.7642 mg/cm^2 for an oxidation treatment of 20 minutes at 850°C. Similarly, Dong et al[4] report increased oxygen diffusion movement rates at higher oxidation treatment temperatures. The hardness increase in the metal below the oxide layer is directly related to the rate of oxygen accumulation. The hardness results, as seen in Figure 16, show that even after three hours of oxidation at 650°C the hardness profile for treatment 650/3 is still well below that of treatment 850/0.5. Both the magnitude and depth of hardening at 650°C was much lower than for the oxidation treatments at 850°C (Figure 16) clearly demonstrating the influence of the lower diffusion movement rate that is a function of treatment temperature[4].

4.1.4 Oxygen diffusion as a function of treatment time

By increasing treatment time, thicker oxide layer growth and deeper diffusion hardening is expected. The increased oxide layer thickness, as a function of treatment time at constant temperature, is clearly seen when comparing Figure 17 and Figure 18 (6 hours vs. 30 minutes at 850°C) and to a much lesser extent when comparing Figure 19 and Figure 20 (3 hours vs. 45 minutes) due to the lower diffusion rate.

Dong et al[4] found that for longer oxidation time at 850°C the weight gain of specimens increased. They showed with a fractograph the lamellar oxide formed after 20, 5 hours. Extensive oxide layer thickening as well as increased diffusion hardening can occur in the extended time period at 850°C. Borgioli et al[28] showed that at 900°C the diffused zone below the oxide layer deepened from 14.1 ± 0.4 µm to 23.5 ± 0.7 µm, when the oxidation time was lengthened from 30 minutes to 2 hours.

The diffused zone reported is the metal under the oxide layer that contains dissolved oxygen.

However, the hardness profiles for the oxidation treatments 650/0.75 and 650/3 (Figure 16) were similar in hardness and hardening depth. Both treatments were conducted at 650^{o}C for different lengths of time. The difference in diffusion hardening between the two specimens oxidised at 650^{o}C would be expected to be very slight and very close to the interface due to the low rate of diffusion movement. The hardness profiles measured at a distance of 20 µm from the interface did not show a difference between oxidation treatments 650/0.75 and 650/3. Guleryuz et al[2] showed that a specimen oxidised at 600^{o}C for 60 hours had showed high diffusion hardening very close to the interface (1 µm = 1250 $HV_{0.005}$) with a hardening depth of 20 µm from the interface, illustrating the shallow hardening at lower diffusion rates at low treatment temperature.

4.2 Preliminary boost diffusion experiment

The hardening results in this section were also obtained using a microhardness tester, by making five indents using 50 gram force at distances of 20, 45, 70, 100, 130, 160, 200 and 300 µm from the interface. The average value for each distance increment was calculated and error bars plotted to show the highest and lowest hardness values below the average.

Step 2 of the OBDH process is referred to as the boost diffusion step during which oxygen dissociates out of the TiO_2 at the interface and into the metal at the interface. Any discontinuities at the interface obstruct oxygen movement into the metal, therefore, interface integrity is crucial for optimum boost diffusion hardening during step 2. This boost diffusion movement causes oxygen to move further from the interface than during step 1 thereby increasing the hardening magnitude as well as depth as is illustrated by comparing the hardness profiles for treatments 650/3 (step 1) and 650/3/Ar (step 2).

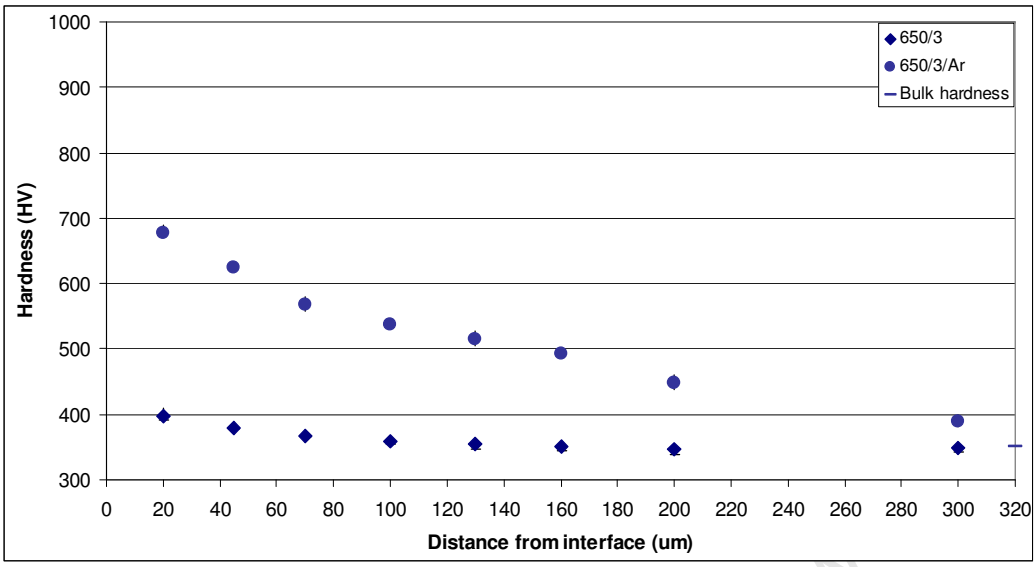

Figure 21: Comparative microhardness profiles for treatments 650/3 and 650/3/Ar illustrating the effectiveness of boost diffusion.

The hardness profile for the oxidation treatment 650/3 in figure 21 illustrates that hardening occurs to a depth of 70 µm while hardening during boost diffusion treatment 650/3/Ar occurs to a depth of 300 µm from the interface. It can also be seen by the vertical distance between the two profiles that the hardness closer than 300 µm from the interface increased in magnitude during step 2.

4.2.1 Boost diffusion in argon

All specimens produced in the preliminary oxidation treatments discussed in section 4.1.1 were subjected to the boost diffusion step in an argon environment for 20 hours at 850°C. This experiment was conducted to determine which oxidation treatment enabled the best boost diffusion hardening during step 2. In this way further information regarding the quality of the oxygen reservoir and its role in the boost diffusion mechanism could be inferred. The following figure shows the hardness profiles obtained from hardness test results from boost diffusion treatments 650/0.75/Ar, 650/3/Ar, 850/6/Ar and 850/0.5/Ar.

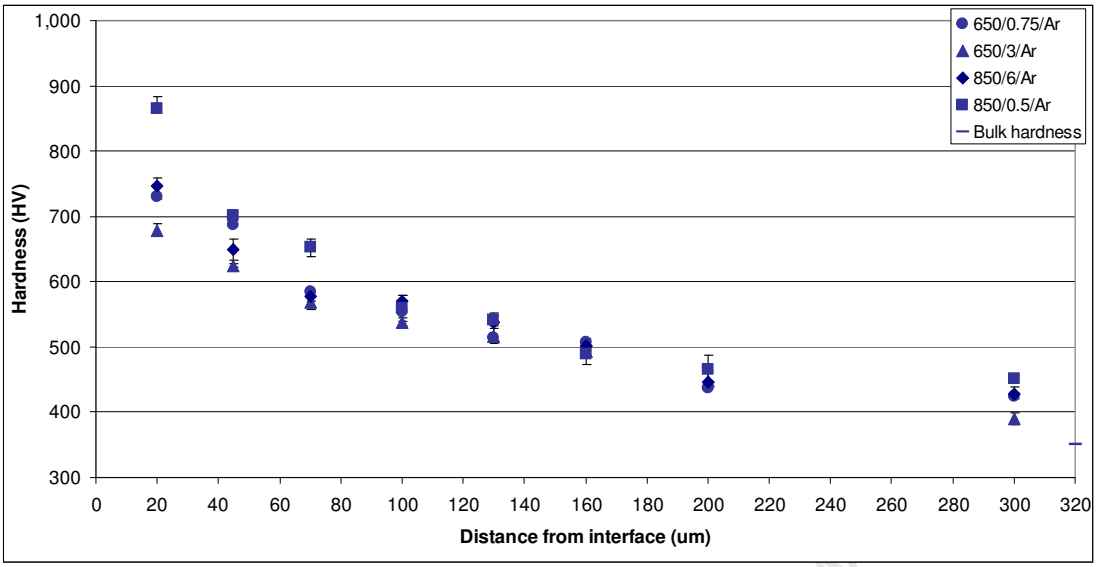

Figure 22: Comparative microhardness profiles for preliminary boost diffusion experiment treatments.

The highest increase in boost diffusion hardening close to the interface was achieved by treatment 850/0.5/Ar (Figure 22), followed by 850/6/Ar and 650/0.75/Ar which had similar hardness values, followed by 650/3/Ar. This order from highest to lowest is seen at a distance of 20 µm from the interface. At a distance of 100 µm – 300 µm from the interface the boost diffusion hardness values are very similar indicating that the depth of the boost diffusion hardened zone is similar in all cases.

The comparison of the hardness profiles for boost diffusion treatments 650/0.75/Ar and 650/3/Ar (Figure 22), reveals slightly higher hardening during treatment 650/0.75/Ar close to the interface. The boost diffusion steps were identical and in Figure 19 and Figure 20 the oxide layer thickness for treatment 650/0.75/Ar was observed to be slightly thinner (2 µm vs. 3 µm) with better interface integrity compared to that of treatment 650/3/Ar. Even though the difference in hardening and oxide layer thickness after step 1 is very small the conclusion is made that even at the lower boost diffusion rate at treatment temperature of 650^{o}C interface integrity can deteriorate and influence the boost diffusion movement and resultant hardening during step 2.

The following two figures (Figure 23 and Figure 24) contain the hardness profiles for step 1 and step 2 for treatments 850/6/Ar and 850/0.5/Ar. By comparing the profiles for the two steps for both treatments, the increased hardening that occurs during the boost diffusion step can be seen. The same set of axes is used to plot the hardness profiles on to make such comparisons possible.

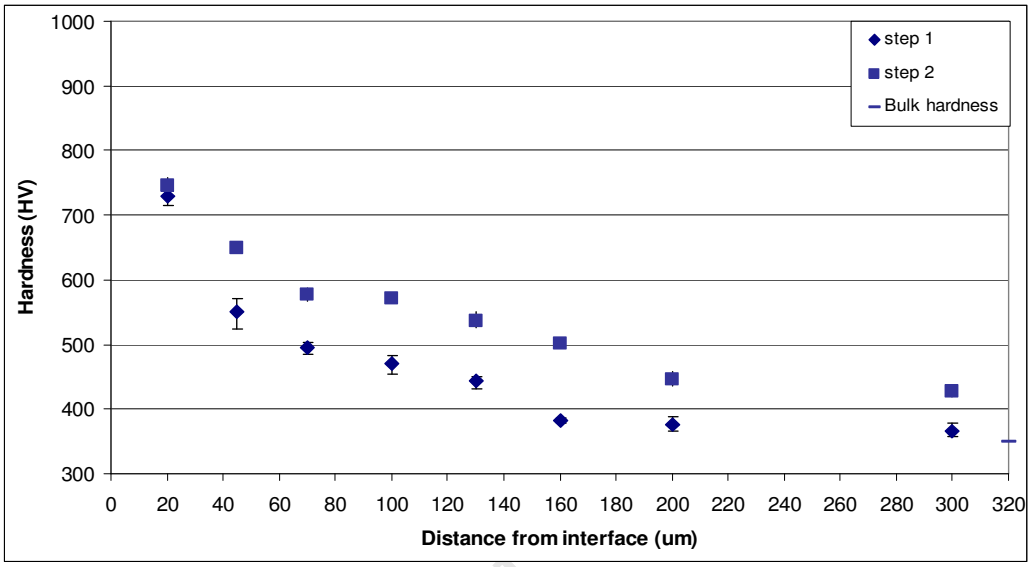

Figure 23: Comparative microhardness profiles illustrating the increase in hardness after step 1 during step 2 of treatment 850/6/Ar.

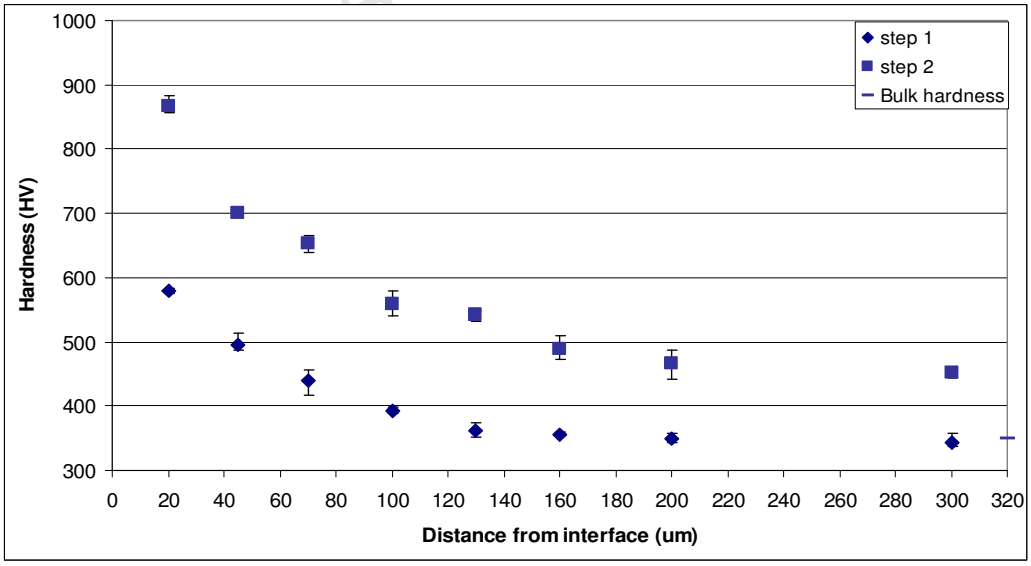

Figure 24: Comparative microhardness profiles illustrating the increase in hardness after step 1 during step 2 of treatment 850/0.5/Ar.

The increase in hardness during boost diffusion treatment 850/0.5/Ar in Figure 24 is greater than the hardness increase during the boost diffusion treatment 850/6/Ar (Figure 23). This increase is seen as the vertical distances between the hardness profiles for step 1 and step 2 for the two treatments. The images in Figure 17 and Figure 18 showed that the interface integrity for treatment 850/0.5 was good while separation of the oxide layer at the interface could be seen for treatment 850/6. The hardness profile comparison in Figure 16 showed that the increased hardness during treatment 850/6 was greater than that of treatment 850/0.5. These results demonstrate that optimisation of boost diffusion can only be achieved when good interface integrity of an oxide layer of optimal thickness exists after step 1 regardless of the diffusion hardening that was achieved during the oxidation step.

4.2.2 Boost diffusion under vacuum

Boost diffusion treatments were also performed under vacuum of 10^{-4}Torr for 20 hours at 850^{o}C and the hardening results compared to that of the OBDH treatments performed in an argon environment. The purpose of this study was to determine whether high vacuum is needed for boost diffusion to occur and whether the boost diffusion can be optimised under high vacuum or in an argon environment.

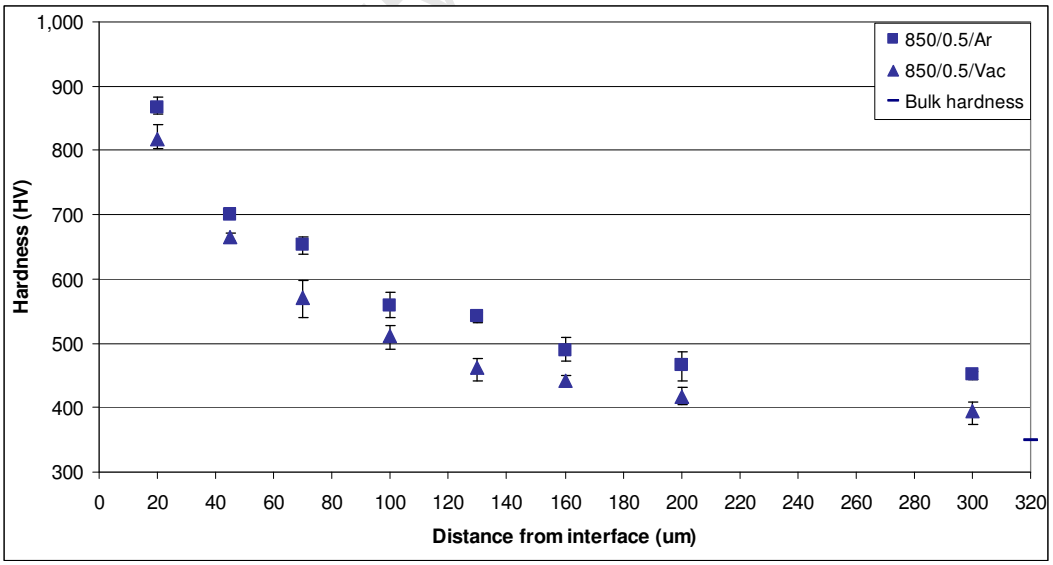

Figure 25: Comparative microhardness profiles of the boost diffusion treatments 850/0.5/Ar and 850/0.5/Vac.

The comparison of the hardness profiles in Figure 25 illustrates that appropriate boost diffusion hardening can be achieved in either environment for step 2. The boost diffusion hardening during the boost diffusion treatment conducted in an argon environment is in this case slightly higher than that for the treatment conducted under vacuum. Zhang et al[3] suggest that high vacuum is crucial for boost diffusion to occur. The results from Figure 25 however contradict this finding illustrating that it is not high vacuum that causes boost diffusion to occur but rather the absence of oxygen in the treatment chamber.

4.3 Oxidation medium experiment

From the results obtained from the preliminary oxidation and boost diffusion experiments (sections 4.1 and 4.2) and reviewed literature[4], the optimum oxidation time and temperature used for step 1 in the following experiments was 30 minutes and 850^{o}C. The furnace heating and cooling rate was 5^{o}C/minute in all cases. Refinement of step 1 treatment conditions was done to optimise boost diffusion by improving the oxide layer quality and interface integrity. Table 8 shows the different oxidation medium conditions used for oxidation treatments in this experiment.

Treatment	**Temperature (^{o}C)**	**Oxidation time (minutes)**	**Oxidation medium**	**Type of gas flow**
Box furnace	850	30	Natural air	Stagnant air
Pulsed O_2	850	30	Pure oxygen	3 x 1 minute pulse
Pulsed MA	850	30	Medical air	3 x 1 minute pulse
CF MA	850	30	Medical air	Continuous

Table 8: Oxidation medium experiment treatment parameters.

4.3.1 Oxide appearance

The following diagrams illustrate the oxide appearance of specimens oxidised under different flow conditions of different oxidising mediums:

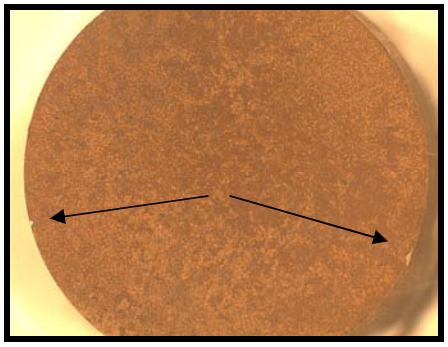

Figure 26: Oxide appearance after treatment Box furnace.

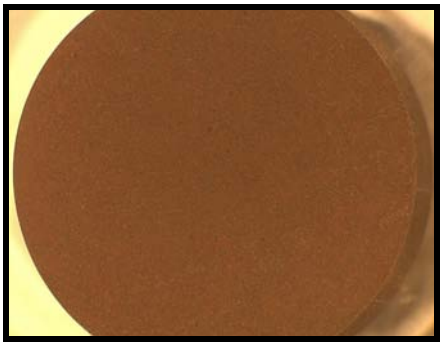

Figure 28: Oxide appearance after treatment Pulsed O_2.

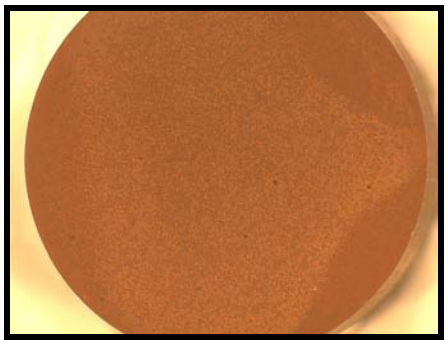

Figure 27: Oxide appearance after treatment CF MA.

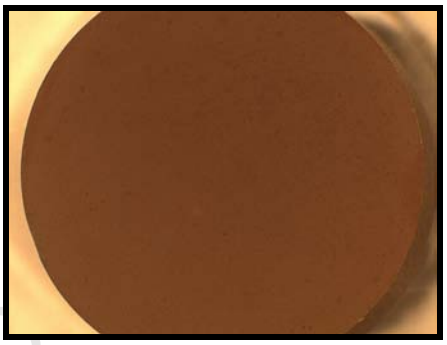

Figure 29: Oxide appearance after treatment Pulsed MA.

The oxide layer formed during the box furnace oxidation treatment in Figure 26 has a mottled appearance. Delamination of the oxide layer from the underlying metal can be seen on the bottom right and left edges of the specimen as is indicated by the arrows. In Figure 27 which indicates the oxide layer on the specimen oxidised in medical air under continuous gas flow conditions, a clear flow direction can be seen in the colouration on the right hand side of the specimen. These flow areas are darker in colour compared to the rest of the specimen surface which has a mottled appearance. In Figure 28 and Figure 29 the colouration for the specimens oxidised under pulsed gas flow conditions is far more even in comparison to the box furnace oxidised specimen. No flow lines are visible and no delamination of the oxide layer from the specimens can be seen in these images.

4.3.2 Oxidation medium hardening results

Microhardness measurements, using 50 gram force, were conducted on the oxidised specimens to compare the diffusion hardening achieved during different oxidising medium experiments conducted at 850°C for 30 minutes. Five indents were made 20, 40, 60, 80 and 100 µm from the interface and the average hardness values calculated and plotted with error bars to show the maximum and minimum hardness values from the average. The nanohardness results, measured as close as possible to the interface, using 5 gram force, were also plotted.

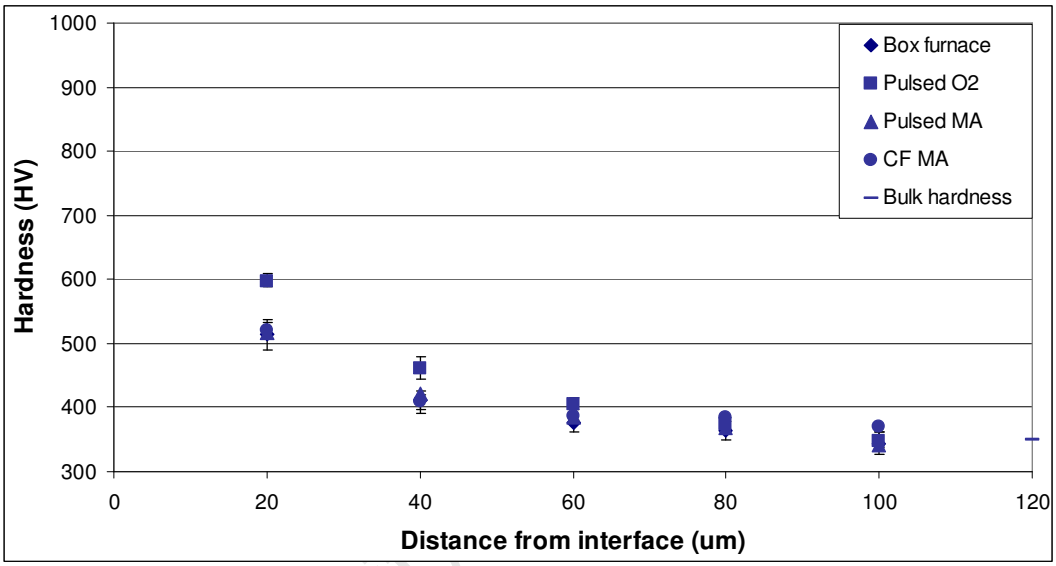

Figure 30: Comparative microhardness profiles for varying oxidising medium oxidation treatments.

From the comparison, as seen in Figure 30, the highest increase in diffusion hardening was achieved during treatment Pulsed O_2. The hardness profiles for the remaining three treatments coincide. Hardening of the metal during all four treatments is seen to occur to a depth of 40 µm from the interface.

The hardening that occurred closer than 30 µm from the interface is shown in the following comparative nanohardness profile plot (Figure 31).

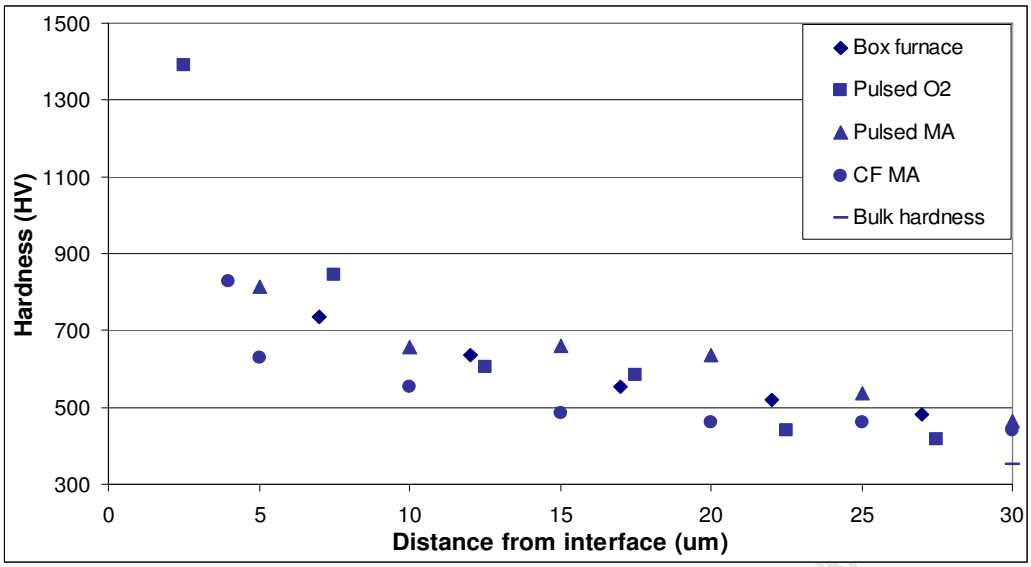

Figure 31: Comparative nanohardness profiles illustrating the diffusion hardening very close to the interface for the oxidation medium experiment treatments.

From the nanohardness profiles, in Figure 31, very little difference in hardness was observed between the hardness profiles for the different treatments.

4.3.3 Surface integrity

It was concluded in section 4.2.1 that the magnitude and depth of hardening will increase through boost diffusion during step 2 regardless of the diffusion hardening that occurred during step 1, provided that an oxygen reservoir of optimum thickness is available with good interface integrity. Optical light microscopy was utilised to compare the oxide layer, interface and underlying metal regions to determine the interface integrity and oxide layer thickness for each of the four oxidation medium treatments. The thickness of the oxide layer that was formed during treatment Box furnace was measured to be in the order of 10 µm and no separation of the oxide layer at the interface is observed.

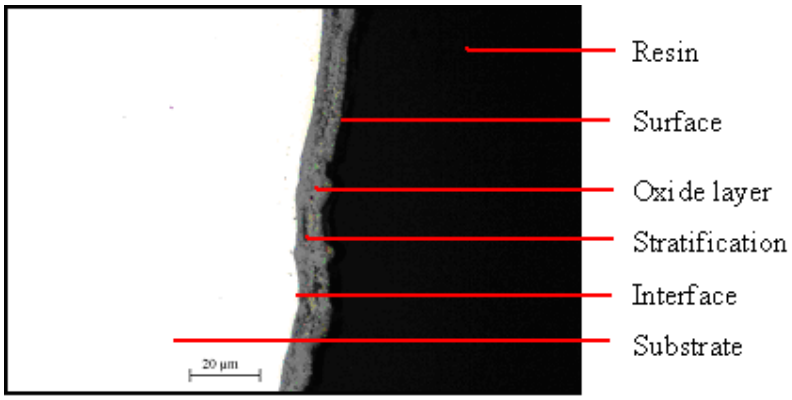

Figure 32: Oxide layer formed during the oxidation in air, for treatment Box furnace.

The oxide layer formed during the oxidation treatment CF MA in Figure 33 has a thickness in the order of 8 µm and no delamination of the oxide layer at the interface observed although some stratification within the oxide layer was observed and is labelled in the image.

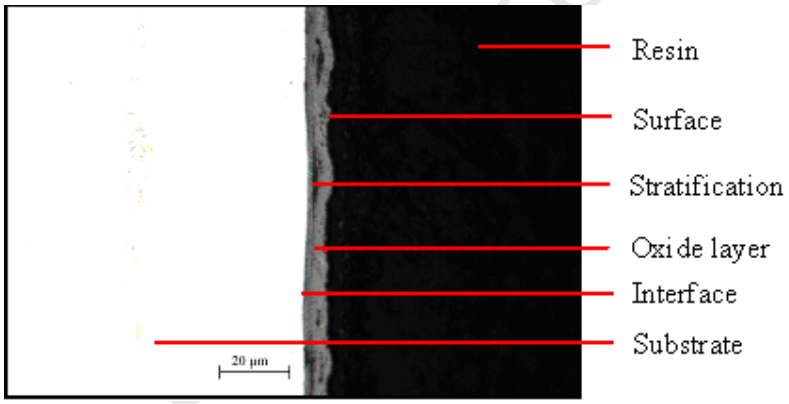

Figure 33: Oxide layer for the continuous medical air flow oxidation treatment CF MA.

The oxide layer formed during the pulsed medical air oxidation treatment is seen in Figure 34. The oxide layer thickness varies between 10 and 12 µm in thickness. Stratification of the oxide layer was observed and is labelled in the figure.

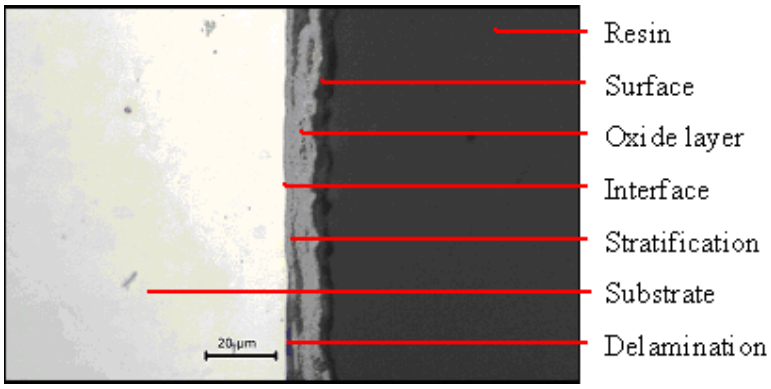

Figure 34: Interface integrity and oxide layer for the pulsed medical air treatment Pulsed MA.

From Figure 35 below the oxide layer treatment O_2 Pulse is seen to have a thickness in the order of 12 µm. No separation is observed within the oxide layer or between the oxide layer and the underlying metal at the interface.

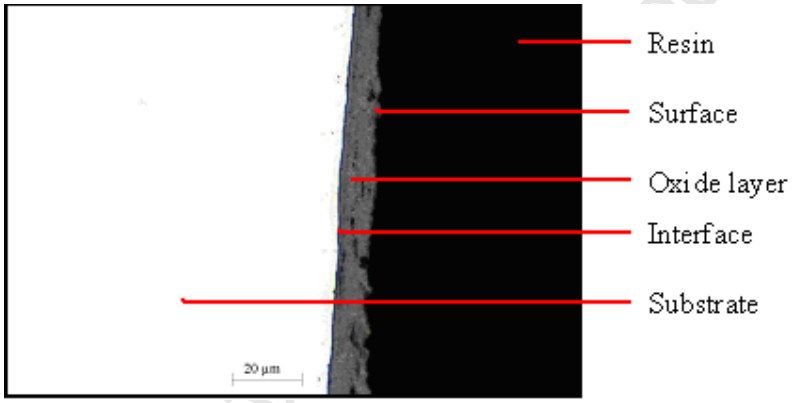

Figure 35: Interface integrity and oxide layer for the pulsed oxygen treatment Pulsed O_2.

Both the microhardness and nanohardness (Figure 30 and Figure 31) results suggest that the largest increased in diffusion hardening was during treatment Pulsed O_2 followed by similar hardening achieved during treatments Pulsed MA, Box furnace and CF MA. This order was also observed in the thicknesses of the oxide layers formed during the oxidation treatments with treatment Pulsed O_2 rendering the thickest (12 µm) most uniform oxide layer followed by a thick (10 – 12 µm) but less uniform oxide layer during treatment Pulsed MA, then the box furnace treatment (10 µm) and lastly the thinner (8 µm) oxide layer formed during treatment CF MA.

Stratification of the oxide layers formed during oxidation treatments conducted in medical air and stagnant air (Box furnace) was observed. During these treatments both oxygen and nitrogen was present in the treatment chamber at the specimen surface for the alloy to react with. The presence of nitrogen during the oxidation step is observed to lower the quality of the oxide layer formed during step 1.

4.4 OBHD hardening experiment

Boost diffusion hardening of specimens heat treated according to the heat treatment matrix (Table 7) was measured as microhardness and nanohardness to determine which treatment conditions result in the highest boost diffusion hardening. By comparing the hardening achieved during these different treatments further understanding of the boost diffusion mechanism was gained in order to optimise the OBDH process.

In this section (4.4) more extensive microhardness measurements were made by measuring the hardening that occurred during treatments at distances of 20, 30, 40, 50, 60, 70, 80, 100, 120, 140, 200 and 300 µm from the interface.

4.4.1 Cyclic vacuum diffusion treatment comparison

The hardness profiles representing the hardening results from three cyclic isothermal treatments with vacuum diffusion steps from the heat treatment matrix are compared in Figure 36 below. The profile for treatment Cyclic/CF O_2/Vac was compiled by calculating the average of five hardness values for each distance increment from the interface while that of treatment Cyclic/Pulsed MA/Vac shows the average hardness value of fifteen indents and that of treatment Cyclic/Pulsed O_2/Vac the average of 30 hardness values for each increment. The error bars in each case show the highest and lowest values from the average.

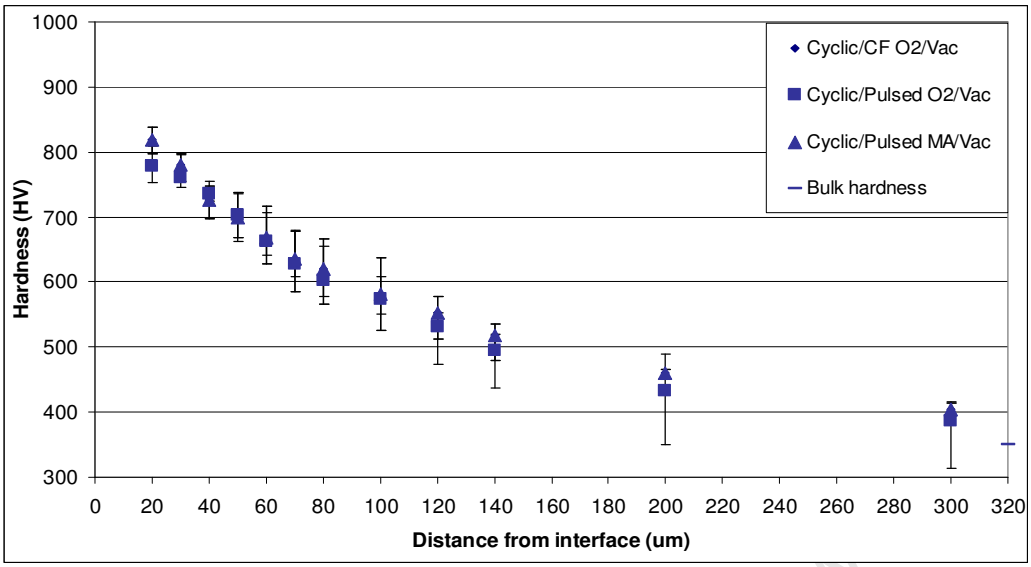

Figure 36: Comparative hardness profiles for three cyclic isothermal treatments with vacuum diffusion steps.

Very similar hardening and depth of hardening occurred during all three treatments: Cyclic/CF O_2/Vac, Cyclic/Pulsed O_2/Vac and Cyclic/Pulsed MA/Vac. The boost diffusion environment and thermal profile for these cyclic treatments were identical while only the oxidation step of each treatment was different in oxidation medium and type of gas flow. As all other treatment parameters were identical, the result shows that different oxidation step conditions during cyclic isothermal treatments do not result in different boost diffusion hardening. During the design of the cyclic OBDH treatments, it was argued that interrupted oxide formation would result in less strain at the interface, which, during isothermal treatments is caused by oxide layer thickness. The light microscope images (section 4.3.3) of the oxide layers formed during the oxidation medium experiments showed notable differences between oxide layer thickness and interface integrity of the formed layers during a continuous oxidation step of 30 minutes at 850^{o}C. From the results obtained from the preliminary boost diffusion experiments it was found that the oxide layer thickness and integrity influences the final achievable hardening during step 2 (section 4.2.1). There is very little difference between the microhardness profiles in Figure 36 illustrating that similar hardening is achieved during all three cyclic isothermal treatments. Despite the assumptions made that the pulsed oxygen treatment could provide a more effective oxygen reservoir the trend in Figure 36 indicates that the boost diffusion step

is not sensitive to the different oxidation steps in this case. The same hardening results can therefore be achieved during three cyclic isothermal OBDH treatments regardless of the oxidation medium and gas flow utilised during the cyclic oxidation steps.

4.4.2 Interrupted thermal vacuum diffusion

The boost diffusion hardening for four interrupted thermal treatments from the heat treatment matrix was measured and the hardness profiles compared in the following figure. Each data point in the hardness profiles for treatments CF O_2/cool/Vac, CF MA/cool/Vac and Pulsed MA/cool/Vac represent the average of five hardness measurements for that distance while the profile for treatment Pulsed O_2/cool/Vac shows the average of 30 hardness values. For each profile the error bars show the highest and lowest value about the average.

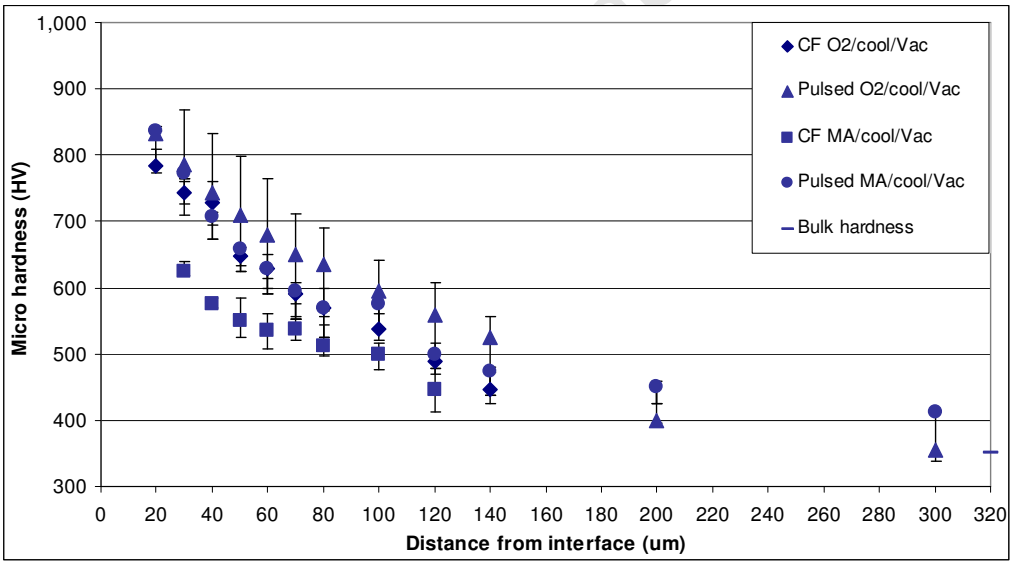

Figure 37: Comparative microhardness profiles for the interrupted thermal vacuum diffusion OBDH treatments.

These treatments had identical thermal profiles which included cooling to room temperature after step 1. Step 2 was performed under a high vacuum environment. The difference between the treatments was the oxidation medium and gas flow during step 1. Although the hardening for the Pulsed O_2/cool/Vac is similar to that of

treatments CF O_2/cool/Vac and Pulsed MA/cool/Vac the results do suggest that treatment Pulsed O_2/cool/Vac has slightly higher hardening while treatment CF MA/cool/Vac achieved the lowest hardening. This is consistent with the comparison of the diffusion hardening during the oxidation medium experiments in Figure 30, which suggested that slightly higher hardening was achieved during the oxidation treatment Pulsed O_2. The comparison between the optical light microscope images (section 4.3.3) of the oxide layers formed during the oxidation medium experiments showed that treatment Pulsed O_2 resulted in the thickest oxide layer with the best adherence, while a thin oxide layer with good adherence but with some stratification within the layer formed during oxidation treatment MA CF. The comparative hardness profiles of the interrupted thermal vacuum treatments in Figure 37 suggest that the thickness and adherence of the oxide layer formed during step 1 influences the final boost diffusion hardening during step 2.

4.4.3 Modification of heat treatment Pulsed O_2/Vac

The microhardness profiles shown in this section (4.4.3) were calculated from 30 hardness values for each distance with error bars indicating the maximum and minimum hardness values about the average.

4.4.3.2 Comparison of Pulsed O_2 vacuum treatments

The microhardness results for three OBDH processes from three treatments with Pulsed O_2 during step 1 and vacuum boost diffusion during step 2 in the heat treatment matrix (Table 7) were compared. These treatments were different in thermal profile and nature of oxidation step and were compared to determine the influence of these differences on the boost diffusion hardening. The treatments were: Pulsed O_2/Vac, Cyclic/Pulsed O_2/Vac and Pulsed O_2/cool/Vac, during which step 1 was conducted under pulsed oxygen conditions and step 2 conducted under high vacuum at 850^{o}C. This comparison was made by plotting the hardness profiles for each of the three treatments on the same axes.

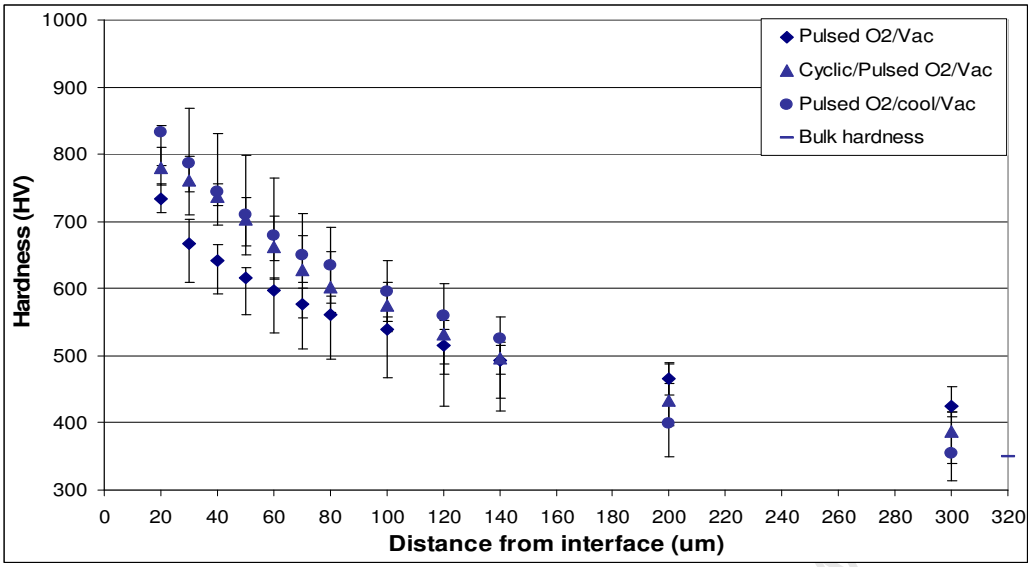

Figure 38: Microhardness profile comparison for treatments Cyclic/Pulsed O_2/Vac, Pulsed O_2/Vac and Pulsed O_2/cool/Vac.

From Figure 38, it was found that the increase in hardness after boost diffusion treatment Cyclic/Pulsed O_2/Vac was greater than for boost diffusion treatment Pulsed O_2/Vac up to 100 µm from the interface. During treatment Cyclic/ Pulsed O_2/Vac the oxidation step was conducted for 10 minutes followed immediately by 6.5 hours of boost diffusion after which two more cycles of oxidation and boost diffusion was conducted. However, during treatment Pulsed O_2/Vac specimens were oxidised for a total time of 30 minutes followed by 20 hours of boost diffusion without any discontinuity in treatment temperature (cooling) between steps.

During the refinement of the OBDH process it was argued that for equivalent treatment time higher hardening would be achieved during cyclic OBDH treatments as compared to that of interrupted thermal treatments which included cooling to room temperature after step 1. This was however not seen in the comparison between the hardness profiles for treatments Cyclic/Pulsed O_2/Vac and Pulsed O_2/cool/Vac; the hardening in fact was similar for the two treatments.

Similarly, during this refinement process continuous isothermal treatments were expected to achieve increased hardening relative to interrupted thermal treatments (conventional two step treatments with cooling after step 1). This was not seen in

Figure 38; in fact, treatment Pulsed O_2/Vac achieved lower hardening than treatment Pulsed O_2/cool/Vac for treatment times of 30 minutes oxidation and 20 hours of boost diffusion. The only difference between the two treatments being that treatment Pulsed O_2/cool/Vac included cooling after step 1.

To determine why the expected results were not achieved the hypothesis was made that further oxidation occurs during cooling after step 1 during treatment Pulsed O_2/cool/Vac. During cooling the temperature in the treatment chamber drops from 850^{o}C to room temperature at a rate of 5^{o}C/min. Oxidation of titanium can readily occur at temperatures above 600^{o}C. This longer oxidation period facilitates extended oxidation treatment time during which increased diffusion hardening occurs. The following calculation shows the extended time at temperature at which oxygen diffusion movement can still readily occur:

850^{o}C – 600^{o}C = 250^{o}C, Cooling rate = 5^{o}C/minute
250^{o}C / 5^{o}C /min = <u>50 minutes</u>

If this hypothesis were true the hardness values for treatment Pulsed O_2/Vac could be increased by introducing a dwell time immediately following the oxidation step. In other words, the oxidation step would be extended for a longer period without further introduction of oxygen into the furnace chamber. Two different dwell periods were introduced: 30 minutes and 120 minutes. These modified treatments were conducted and repeated and the hardness results compared by plotting the hardness profiles on the same set of axes.

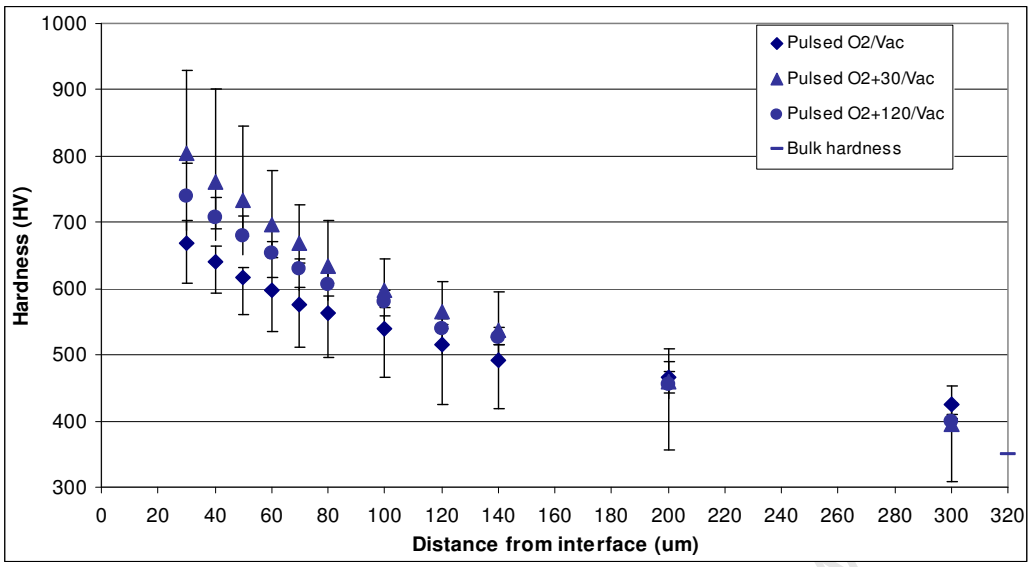

Figure 39: Microhardness profiles for heat treatment Pulsed O_2/Vac and its modifications.

The boost diffusion hardening for treatment Pulsed O_2+30/Vac was slightly higher than that of Pulsed O_2+120/Vac in Figure 39 while the hardness profile for the original treatment lies below those of the modified treatments. These results prove the hypothesis that boost diffusion hardening results can be increased by extending the treatment time during the oxidation of treatment Pulsed O_2/Vac. This observation indicates that treatments that include cooling have longer oxidation treatment step times, implying that the treatment times for the interrupted thermal (cooling between steps) treatment and the isothermal treatments (cyclic and continuous) were not equal.

Even though the hardening for the two modified treatments are quite similar, the results do suggest that the boost diffusion hardening was optimised during treatment Pulsed O_2+30/Vac as opposed to treatment Pulsed O_2+120/Vac. This could be explained by considering the oxide layer adherence after the oxidation step. It was discussed in section 2.2.3.1.2, that delamination of the oxide layer occurs during cooling due to increased thickness. As no cooling occurred during the modified treatments delamination as a result of cooling could not have occurred. The high Pilling-Bedworth ratio of titanium implies that the volume of the formed oxide layer is greater than that for the metal, causing residual stresses that increase with oxide layer thickness. The duration of step 1 of treatment Pulsed O_2+120/Vac was 150

minutes at 850°C. Figure 17 on page 57 shows that the oxide layer formed during oxidation treatment 850/3 (180 minutes at 850°C followed by furnace fooling) was 40 µm thick. Even though no cooling occurred after the extended oxidation time for treatment Pulsed O_2+120/Vac, it is believed that delamination of the oxide layer could have occurred as a result of the large increase in volume due to increased oxide layer thickness. This delamination inhibits boost diffusion movement of oxygen which limits the final achievable boost diffusion hardening.

4.4.3.3 Comparison of Pulsed O_2 vacuum and modified treatments

The boost diffusion hardening increased during the modified treatments Pulsed O_2+30/Vac and Pulsed O_2+120/Vac. The hardness profiles for the modified treatments, the original treatment and treatments Cyclic/Pulsed O_2/Vac and Pulsed O_2/cool/Vac were compared.

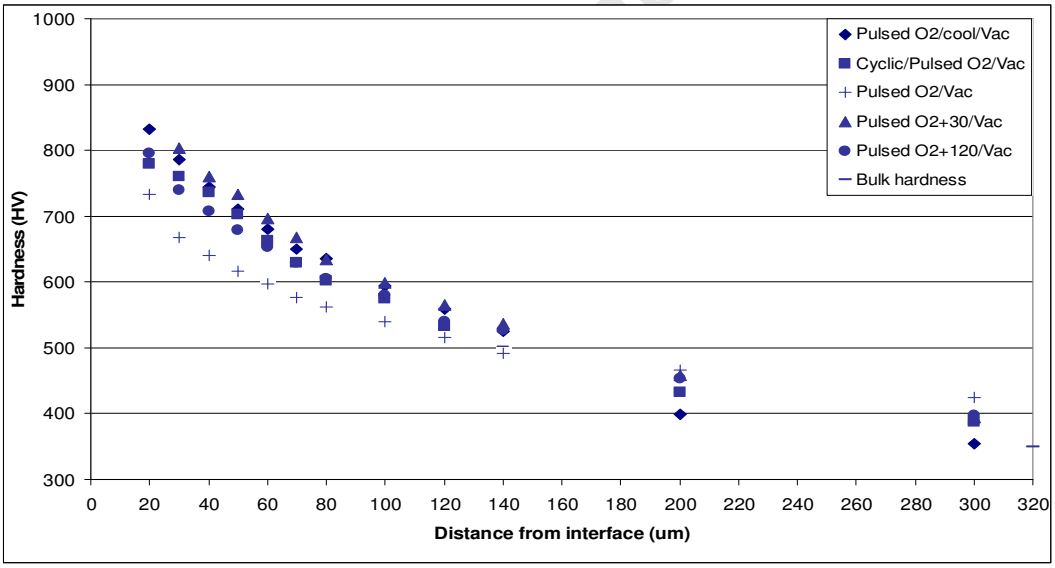

Figure 40: Comparative hardness profiles of Pulsed O_2 vacuum and the modified Pulsed O_2 vacuum boost diffusion treatments.

From the hardness profile comparison in Figure 40 it was found that treatment Pulsed O_2+30/Vac resulted in the highest hardening followed closely by Pulsed O_2/cool/Vac then by treatment Cyclic/Pulsed O_2/Vac and then Pulsed O_2+120/Vac. The profile for treatment Pulsed O_2/Vac was the lowest of all the treatments. Consequently, it may

be stated that appropriate boost diffusion hardening could be achieved by four different OBDH processes.

To determine which of the treatments that yielded similar boost diffusion hardening was the most efficient the total treatment time was calculated and compared. The Ti-6Al-4V alloy is known to react readily with oxygen at temperatures above 600^{o}C[6,7,33]. The total time at temperatures above 600^{o}C between the start of step 1 and the end of step 2 during treatments was compared in the following table:

Treatment	Step 1 (minutes)	Step 2 (hours)	Cooling or dwell time (minutes)	Total time at temp (hours)
Pulsed O_2+30/Vac	30	20	30	21
Pulsed O_2+120/Vac	30	20	120	22,5
Cyclic/Pulsed O_2/Vac	30	19,5	0	20
Pulsed O_2/cool/Vac	30	20	50	21,33

Table 9: Cumulative total treatment times for treatments with similar hardening results.

From the comparison made between the treatment time at temperature it was found that similar hardening could be achieved through treatments for which the treatment times were not equal. The shortest time at temperature was during boost diffusion treatment Cyclic/Pulsed O_2/Vac followed by treatment Pulsed O_2+30/Vac and then treatment Pulsed O_2/cool/Vac and finally Pulsed O_2+120/Vac. The shortest total treatment time at temperature to appropriate boost diffusion hardening was therefore 20 hours during treatment Cyclic/Pulsed O_2/Vac.

4.4.4 Boost diffusion medium

It was concluded in section 4.2.2 that similar boost diffusion hardening can be achieved during treatments for which only the boost diffusion environment is different. In the following diagram the micro- and nanohardness results were combined to create a single hardness profile for each treatment, namely; Pulsed O_2/cool/Ar and Pulsed O_2/cool/Vac, very little difference was found in the hardening for both treatments.

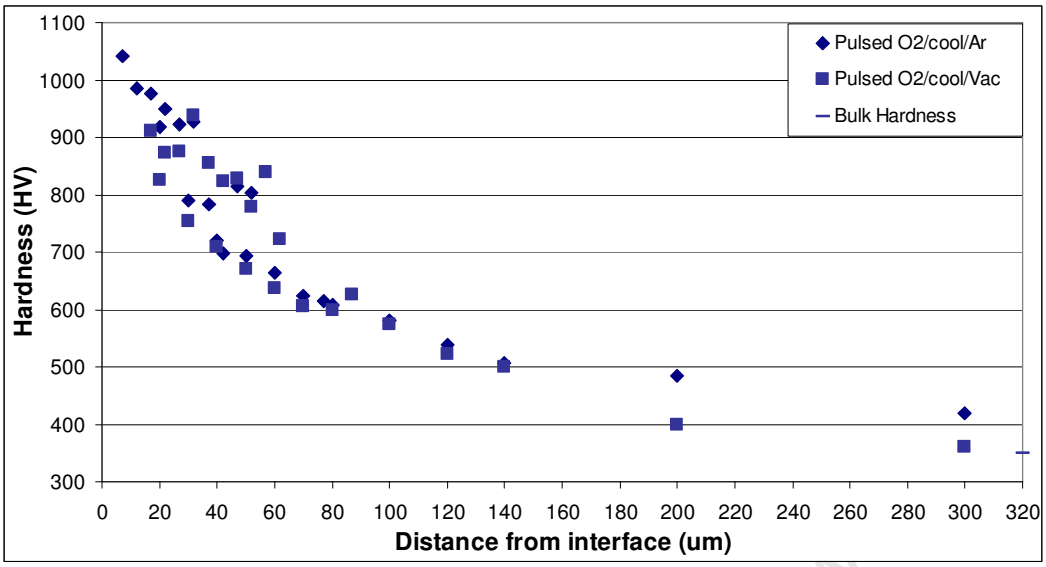

Figure 41: Comparative micro- and nanohardness profiles showing similar boost diffusion hardening in an argon and high vacuum environment.

From the comparison between the hardness profiles for the two treatments seen in figure 41, similar boost diffusion hardening can be achieved through boost diffusion treatments conducted in either an argon environment or under high vacuum. These results reinforce the conclusion that it is not high vacuum that causes boost diffusion to occur but the absence of oxygen in the treatment chamber during step 2 that causes boost diffusion to occur. This result shows that high vacuum is not required for boost diffusion; boost diffusion hardening of titanium alloys could occur in any oxygen free environment.

4.4.5 Nitrogen diffusion

Oxygen and nitrogen atoms are known to diffuse into titanium and can fill the same interstitial positions[4]. The boost diffusion hardening effect of oxygen exceeds that of nitrogen: once diffused into the crystal lattice nitrogen is more reluctant to move to a deeper position, thereby decreasing the boost diffusion hardening. This retardation of oxygen diffusion movement by nitrogen atoms is discussed in section 2.2.7 of the literature review. Dong et al[4] reports a high concentration of nitrogen atoms at the interface by means of a composition profile, referring to it as a nitrogen pile-up (Figure 4 in section 2.2.7). The boost diffusion hardening for a specimen oxidised in

an environment with both oxygen and nitrogen present, such as medical air, is expected to be lower than for a specimen oxidised in pure oxygen. The hardening during treatments that had oxidation steps under oxygen and medical air conditions followed by an identical step 2 were compared.

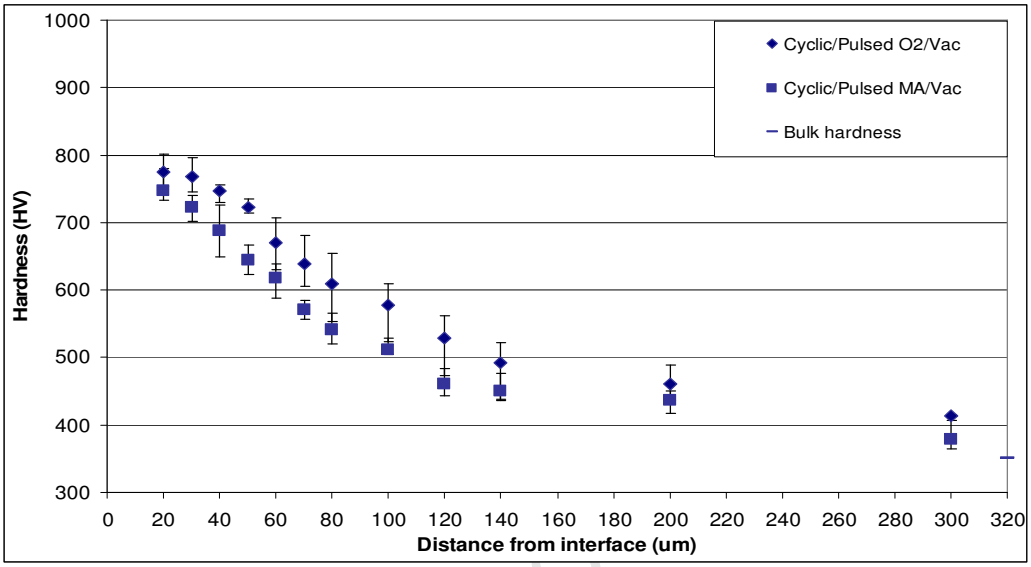

Figure 42: Comparative hardness profiles illustrating the influence of nitrogen during cyclic isothermal boost diffusion treatments.

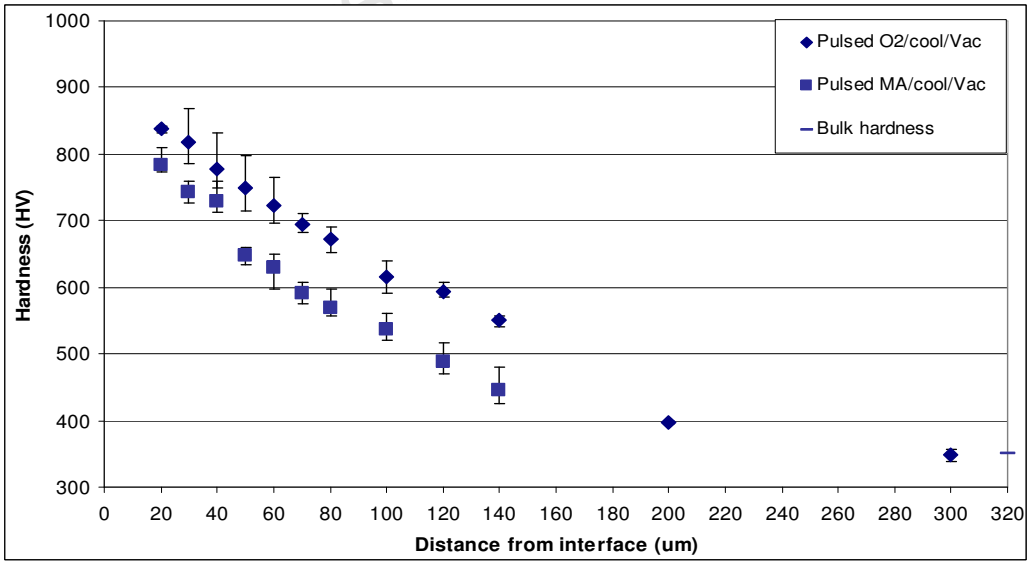

Figure 43: Comparative hardness profiles illustrating the influence of nitrogen during interrupted thermal boost diffusion treatments.

The comparison of the hardness profiles obtained from the cyclic isothermal treatments Cyclic/Pulsed O_2/Vac and Cyclic/Pulsed MA/Vac (Figure 42) show that specimen Cyclic/Pulsed O_2/Vac has higher hardness. This is also seen when the hardness profiles for the conventional two step treatments with cooling between steps, Pulsed O_2/cool/Vac and Pulsed MA/cool/Vac are compared (Figure 43). The comparison between the hardness profiles shows that the increase in hardening during step 2 is greater for specimens that were oxidised in pure oxygen during step 1. The specimens that were oxidised during step 1 in medical air, which contains 79% nitrogen, had a lower final hardness after the boost diffusion step. These results show that nitrogen inhibits the diffusion movement of oxygen atoms into the metal and thereby limits the hardening that occurs during step 2. Greater boost diffusion hardening can therefore be achieved in specimens that have been oxidised in pure oxygen. The optical light microscope images (section 4.3.3) revealed that the oxide layers formed during oxidation steps in both oxygen and nitrogen were of poor quality as stratification could be seen for treatments Box furnace, Pulsed MA and CF MA. Poor oxide layer quality and interface integrity inhibit diffusion movement of oxygen during step 2. Boost diffusion hardening during OBDH processes can therefore be optimised by conducting the step 1 in pure oxygen.

4.5 Clarification of the boost diffusion mechanism

4.5.1 Suggested mechanism for oxide formation

The following diagram gives a description of the oxide formation through diffusion movement of oxygen into titanium metal during the oxidation step:

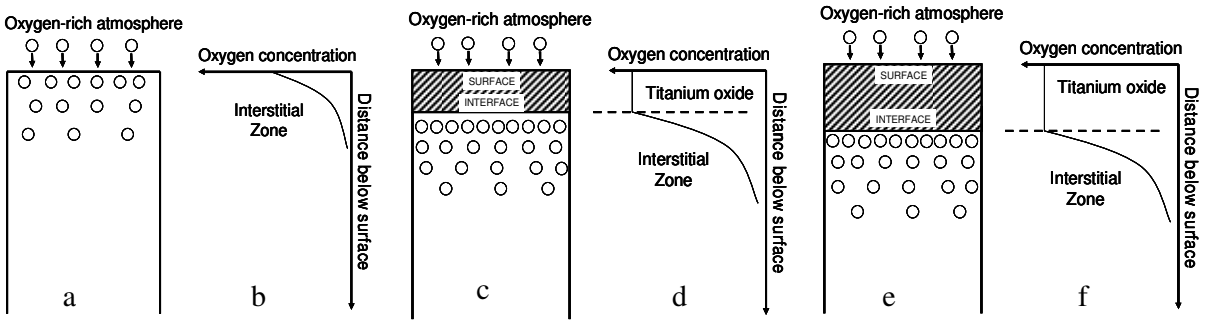

Figure 44: Diffusion movement of oxygen into titanium metal during the oxidation step.

During the oxidation step at elevated temperature, oxygen from the enriched environment dissociates at the metal surface and diffuses into interstitial (octahedral) positions in the microstructure of the titanium metal raising the dissolved oxygen concentration. This movement is illustrated in Figure 44 (a). Figure 44 (b) illustrates the parabolic concentration gradient present in the metal in the zone where oxygen is dissolved interstitially into the metal.

As more oxygen atoms diffuse into the metal, the dissolved oxygen concentration in the metal at the surface builds up and reaches the critical stoichiometric concentration required for TiO_2 formation which is equal to 66,67 atomic %. The oxide formation causes an interface between the oxide and the oxygen rich titanium metal and is illustrated in Figure 44 (c). Figure 44 (d) illustrates the critical oxygen concentration of dissolved oxygen in the TiO_2 layer and the concentration gradient in the interstitial zone below. This TiO_2 layer grows away from the metal surface and into the metal in the direction of oxygen diffusion movement.

The oxide layer does not impede further diffusion movement of oxygen into the metal. Oxygen can, therefore diffuse unhindered through the oxide layer to the interface where it is either utilised for oxide layer growth or increasing the depth of the concentration gradient as seen in Figure 44 (e). In Figure 44 (f) the concentration gradient illustrates the thickness increase of the TiO_2 layer and the increased depth of the interstitial zone.

4.5.2 Microstructural analysis of an oxidised specimen

A combination of SEM and EBSD was utilised to examine the nature of the microstructural changes of oxide layer, interface and underlying metal during the oxidation step of the OBDH process.

4.5.2.1 Oxide layer formation

The SEM image (Figure 45) of the oxide layer formed during oxidation treatment 850/0.5 shows that the oxide layer is as thick as 10 µm, which is consistent with the thickness observed in the light microscope image in Figure 18. As in the light

microscope image, the TiO_2 layer, the interface and the underlying titanium metal can be identified. From the SEM image however, an intermediate layer was observed between the TiO_2 layer and titanium metal. The interface therefore was not between TiO_2 and metal but between this intermediate oxide and the metal. Zang et al[3] used XRD analysis to report on a sub-oxide or intermediate layer that consists of oxygen deprived titanium oxides (section 2.2.3.3).

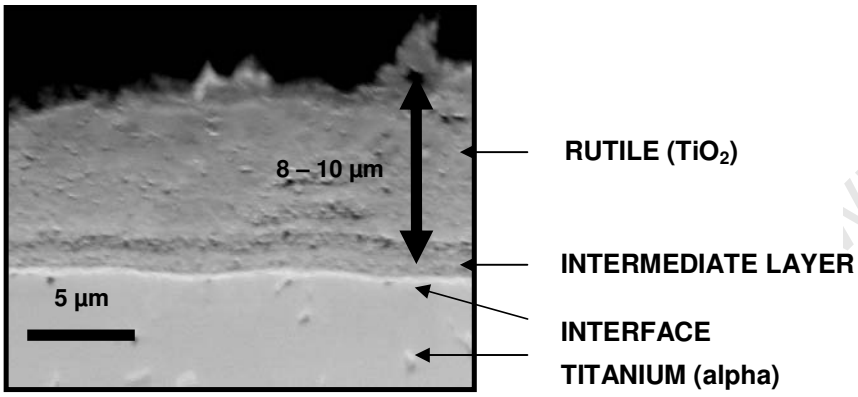

Figure 45: SEM image of the oxide layer formed during oxidation treatment 850/0.5.

Two SEM images of the oxide layer formed during oxidation treatment 850/0.5 are shown in Figure 46. In these images the TiO_2 oxide layer, the underlying metal and the intermediate layer between the rutile layer and the metal are clearly visible. EBSD orientation maps of a region within the oxide layer were imaged from which the grain size distribution of TiO_2 grains in the oxide layer could be determined. The step size utilised during the imaging of the EBSD maps was 0.3 µm for (a) and 0.16 µm for (b). This small step size was utilised to accurately measure the size of the nucleated grains which would not have been possible with a bigger step size. The EBSD images revealed a decrease in TiO_2 grain size from the surface towards the interface. This is shown by the 2 µm diameter grains close to the surface and the 0.5 µm diameter grains closest to the intermediate layer in Figure 46 below.

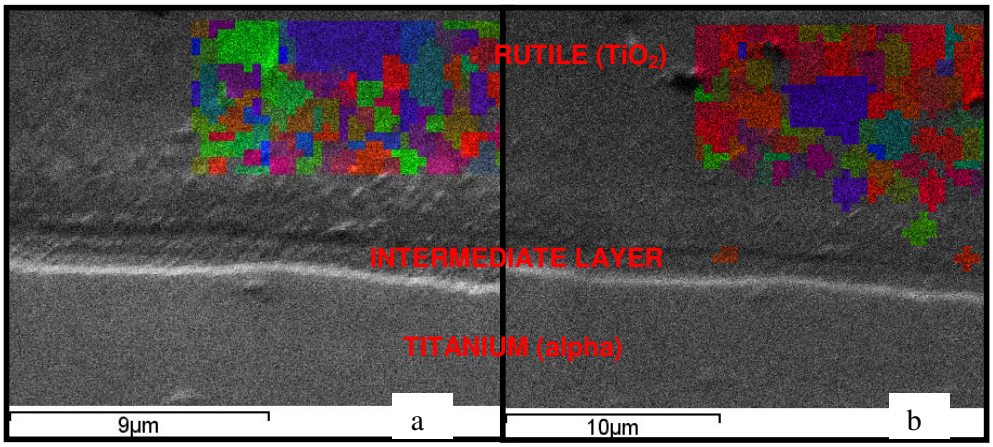

Figure 46: SEM images of the same region showing TiO_2 grain size and orientation after oxidation treatment 850/0.5.

A Zeiss ULTRA 55 FEGSEM was used to obtain the following SEM image of the TiO_2 layer formed during treatment 850/0.5 using an operating voltage of 0.82 kV in Figure 47. In this image the grain size distribution from large (1-2 µm) close to the surface to fine (< 0.5 µm) close to the interface between the TiO_2 grains is observed. Even finer grains are visible in the intermediate layer. The grain size of the underlying titanium α grains in this image are in the order of 10 µm.

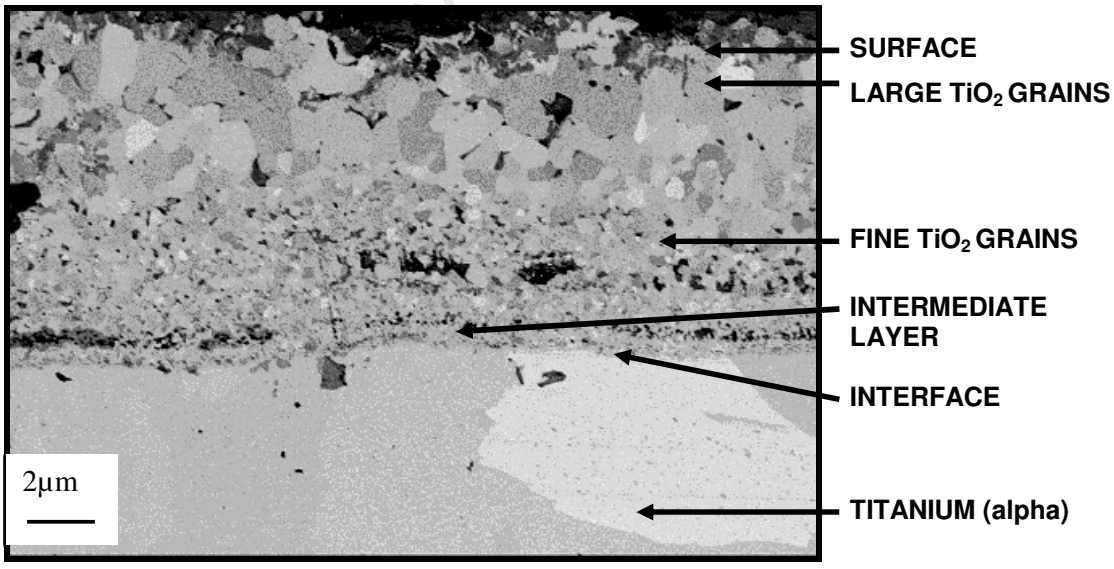

Figure 47: SEM image showing grain size information of the oxide layer formed during oxidation treatment 850/0.5.

The following EBSD map (Figure 48) was imaged using a step size of 0.16 µm and shows the grain size and orientations of the TiO_2 grains as well as the large α titanium grains at the interface below the oxide layer. During the imaging of the EBSD orientation map the software was set to index diffraction patterns for both TiO_2 and α titanium metal and are seen as the coloured grains in the map. The black pixels are plotted where the software could not solve the diffraction pattern generated in those particular positions. This unindexed region coincides with the intermediate layer that has been observed in all the SEM images of the formed oxide layer. This shows that this intermediate layer is not yet TiO_2, but no longer α titanium metal. It is in fact a graded zone with an oxygen concentration that decreases from the stoichiometric concentration for TiO_2 to that of oxygen rich titanium metal. This zone was reported to be an oxygen deprived titanium oxide by Zang et al[3]. The metal below the intermediate layer at the oxide was again indexed as α titanium metal with a grain size in the order of 10 µm.

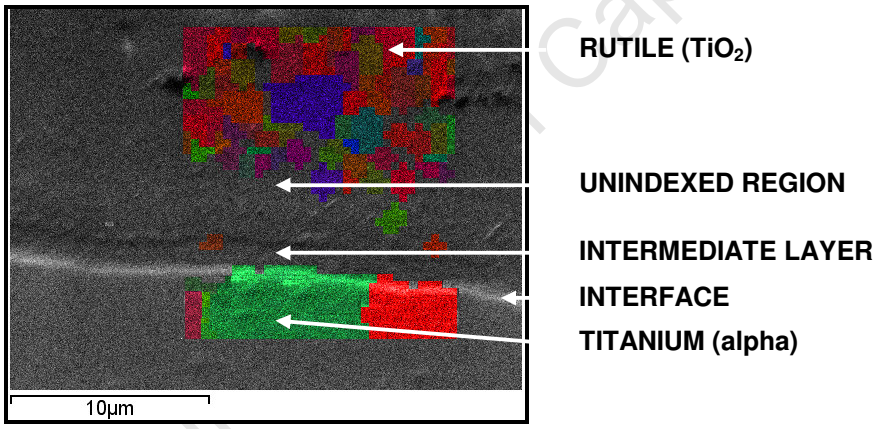

Figure 48: Secondary electron image and EBSD orientation map illustrating the grain size distribution in both the TiO_2 and underlying titanium metal.

The SEM images (Figure 46 - Figure 48) of the oxide layer formed during treatment 850/0.5 show that oxide formation does indeed occur according to the mechanism discussed in section 4.5.1. During the oxidation step the stoichiometric concentration for rutile TiO_2 is reached at the surface where the transformation of titanium metal into TiO_2 occurs through the nucleation of TiO_2 grains. This nucleation continues deeper into the metal in the direction of oxygen diffusion movement. The TiO_2 grains that nucleated first (on the surface) have time to grow during step 1 which is

conducted at 850°C and the oxide layer consequently forms through a nucleation and grain growth mechanism contrary to the epitaxial oxide grain growth reported by Lenarduzzi et al[7]. A region exists between the TiO_2 layer and the underlying metal that has a very high oxygen concentration that is still below the stoichiometric concentration of 66,67 at% but too high for titanium metal to exist. This region is the intermediate layer that will consist of titanium oxides such as TiO, Ti_2O_3 and Ti_4O_7as reported by Zang et al[3].

4.5.2.2 Underlying titanium metal

The EBSD orientation map of the titanium metal directly below the oxide layer formed during treatment 850/0.5 showed that the average grain size was in the order of 10 µm which is consistent with the average grain size observed in the previous images.

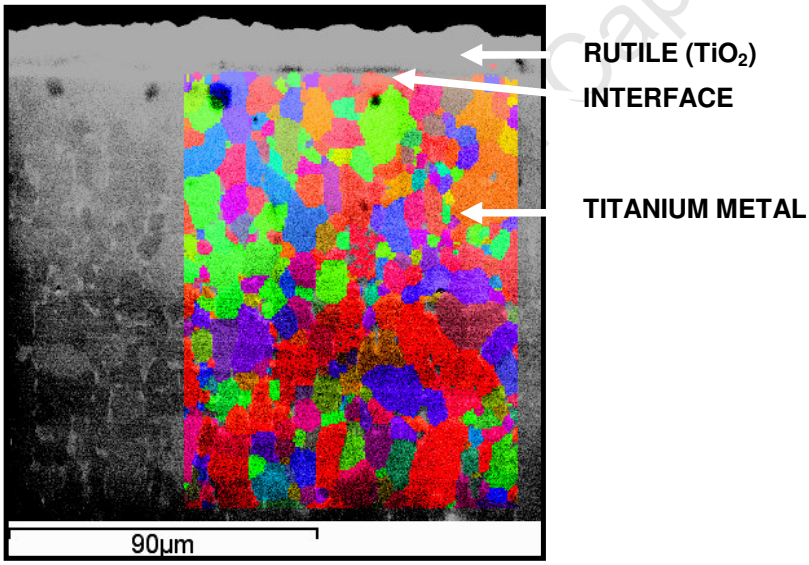

Figure 49: SEM and EBSD images illustrating the average grain size of titanium α grains after oxidation treatment 850/0.5.

An experiment was performed to image the α and β microstructure using EBSD. Figure 49 shows the α grain structure only whereas the distribution of both phases is indicated in Figure 50. The α grains are yellow regardless of size and orientation while β grains are magenta. This image shows that almost no β grains are present in

the 10 µm region below the interface. The occurrence of β grains increases with distance from the interface. This is consistent with the findings of Dong et al[4] who report on the absence of β grains in titanium metal regions with high oxygen concentrations. Oxygen is a strong α phase stabiliser which causes the transformation of β grains into stable α grains in titanium metal with high dissolved oxygen concentrations.

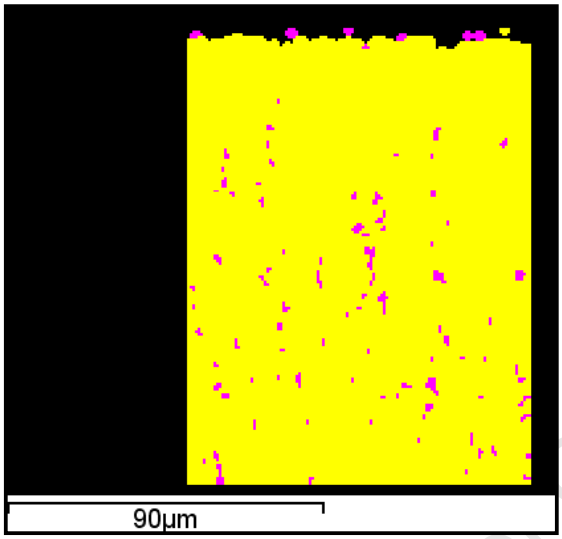

Figure 50: Image showing the occurrence of β grains in the titanium metal after oxidation treatment 850/0.5.

4.5.3 Suggested mechanism for boost diffusion

The second step in the OBDH process is the boost diffusion step. The diagram below illustrates the diffusion movement of oxygen out of the oxide layer and into the metal during step 2, and provides the following description of the boost diffusion mechanism:

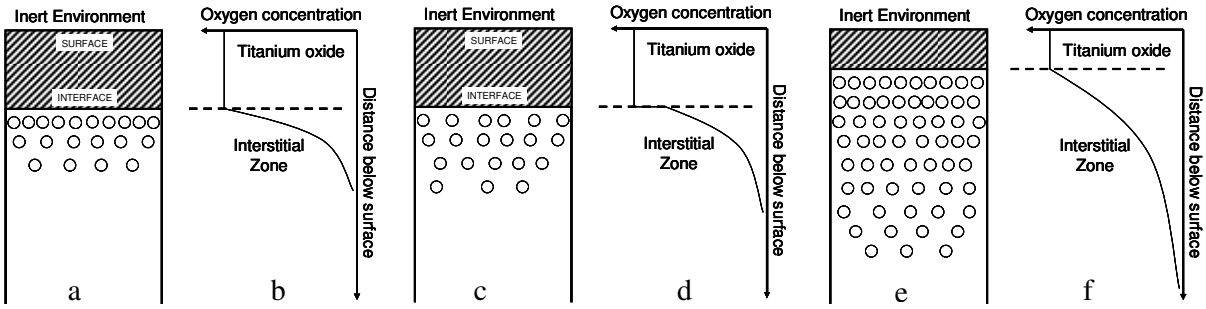

Figure 51: Diffusion movement of oxygen into titanium metal during the boost diffusion step.

The second step of the OBDH treatment is conducted in an oxygen free environment at elevated temperature. During this step there is, therefore, no oxygen present at the specimen surface as seen in Figure 51 (a). Figure 51 (b) illustrates the oxygen concentration of the oxide layer and the concentration gradient of dissolved oxygen in the interstitial zone below the interface.

The driving force for oxygen to diffuse deeper into the metal down the oxygen concentration gradient still exists. This continued diffusion movement causes a drop in oxygen concentration in the metal at the oxide metal interface as illustrated in Figure 51 (c). The concentration gradient in Figure 51 (d) illustrates the discontinuity of oxygen concentration in the metal below the interface caused by the continued diffusion movement of oxygen down the concentration gradient.

This discontinuity in concentration is the driving force for oxygen to dissociate out of titanium oxide at the interface, freeing up oxygen atoms to fill the emptied positions in the metal at the interface. This dissociation lowers the oxygen concentration in the titanium oxide below stoichiometry which implies that the oxide can no longer exist and thereby actively decomposing the oxide layer towards the surface as illustrated in Figure 51 (e). This movement of the interface causes the transformation of titanium oxide into α titanium metal. During this step oxygen is diffused deeper into the substrate as can be seen from the concentration gradient in Figure 51 (f). The oxygen reservoir formed in the first step of the OBDH treatment enables increased oxygen diffusion movement during the second step which is why it is referred to as boost diffusion.

4.5.4 Microstructural analysis of OBDH treated specimens

SEM imaging was conducted on a prepared specimen that had undergone the OBDH process during treatment Pulsed O_2/cool/Vac. Both secondary electron and EBSD images of the near surface region of the specimen were imaged. The EBSD map revealed a refined titanium metal grain structure below the oxide layer with a grain size in the order of 2 µm. Larger titanium α grains were observed below these with grain sizes in the order of 5 µm.

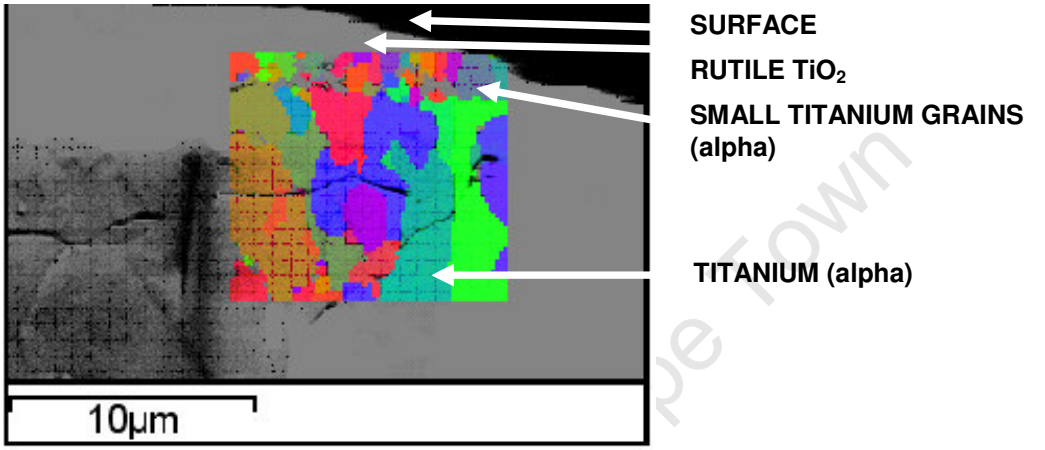

Figure 52: EBSD image illustrating the grain size distribution below the interface after treatment Pulsed O_2/cool/Vac.

A SEM image of the oxide layer and near surface region of a specimen that had undergone the boost diffusion hardening during treatment Pulsed O_2/cool/Vac is shown in the following figure.

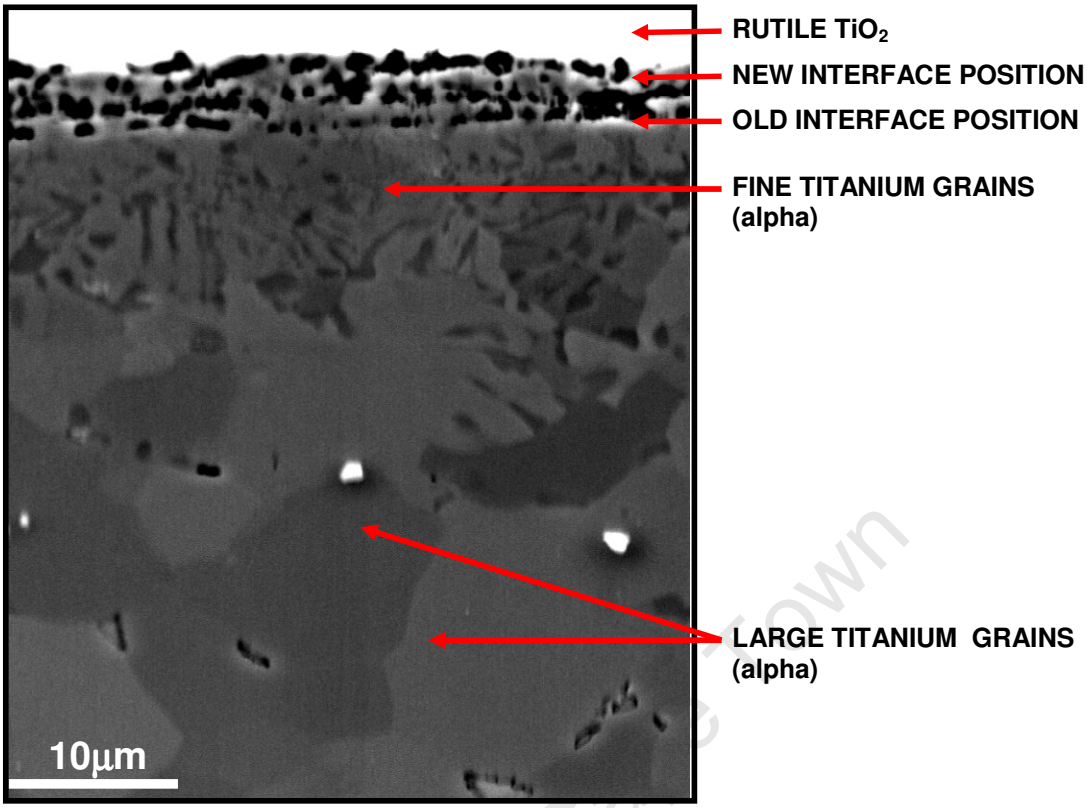

Figure 53: SEM image of the grain structure development during treatment Pulsed O_2/cool/Vac.

The image in Figure 53 shows the region below the oxide layer and illustrates the underlying refined grain structure of the α titanium metal between the old and new interface positions. It also shows grain refinement of the α titanium grains below the old interface position and the large underlying titanium metal grains with grain size in the order of 20 µm. The average grain size of the underlying metal after step 1 was 10 µm illustrating that considerable grain growth of these grains occur during step 2 of the OBDH process.

The following EBSD orientation map (Figure 54) is of the region immediately below the oxide layer and shows the new interface position below the oxide layer as well as the old interface position with nucleated α titanium grains between the two positions. The grain size of the nucleated grains is seen to increase in size from the new interface position in the direction of the old interface position. The image also shows

the refined grain structure below the old interface position. The mechanism for the grain refinement below the old interface position has not been identified.

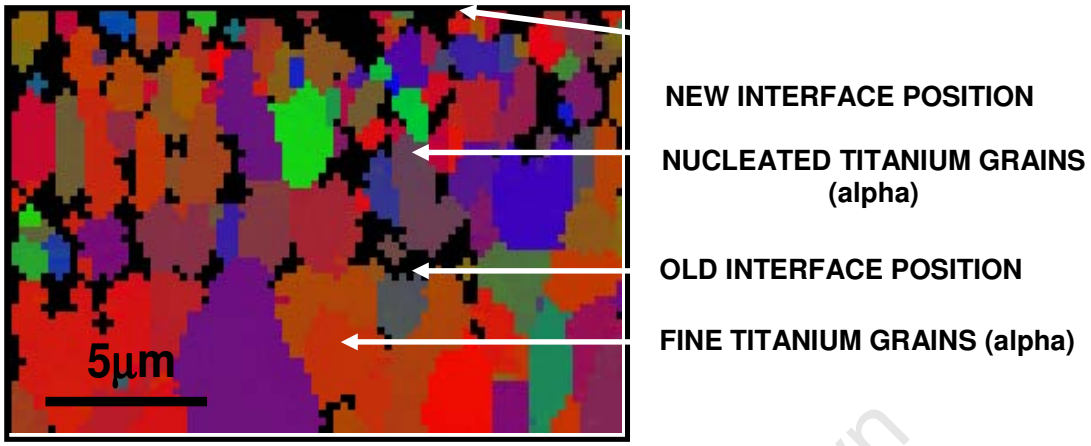

Figure 54: EBSD orientation map of the nucleated titanium metal between the new and old interface positions.

The SEM and EBSD images of the OBDH treated samples revealed that the suggested mechanism for boost diffusion is indeed correct (section 4.5.3). The continued diffusion movement of oxygen down the concentration gradient causes a drop in concentration in the metal at the interface which is the driving force for the decomposition of the oxide at the interface. This decomposition continues towards the surface resulting in the movement of the interface position. Titanium oxide can no longer exist when the oxygen concentration has dropped below stoichiometry and titanium oxide therefore transforms into titanium metal through the nucleation of α titanium grains at the interface and continues toward the surface in the direction of oxide decomposition. During step 2 grain growth of these nucleated α grains occurs. Zang et al[3] reported the presence cracks and pores below the oxide layer. The presence of pores was found in this present study in the region where the nucleation of α titanium metal occurred and can clearly be seen in Figure 53 and Figure 54. This region used to consist of titanium oxide which formed due to the high dissolved oxygen concentration (66,67 at% for TiO_2). Due to the high Pilling- Bedworth ratio of titanium the titanium oxide will have a larger volume than the titanium metal. Therefore porosity now exists when new titanium metal with a smaller volume nucleates in the place of titanium oxide.

Zang et al[3] suggested that the drop in oxygen concentration at the interface during step 2 is caused by the insufficient rate of decomposition of the oxide layer (section 2.2.3.3). This current research shows that the continued diffusion movement down the concentration gradient causes a drop in concentration which is the driving force for the decomposition of the oxide to release oxygen to diffuse into the emptied positions in the metal at the interface.

5 CONCLUSIONS

In order to further optimise the OBDH process several arguments were proposed in this thesis.

(i) It was hypothesised that a continuous isothermal two step treatment with no cooling between steps would eliminate any disruption of the oxide-metal interface that occurs during cooling and reheating of the conventional (interrupted thermal) two step OBDH process that includes cooling after step 1. The isothermal treatments would maintain higher interface integrity. Hence these treatments would achieve more effective boost diffusion hardening than the conventional two step process.

- Continuous isothermal treatments achieved lower boost diffusion results than the interrupted thermal treatments which included cooling.

- It was found that longer time for oxide formation was available during the cooling period after the oxidation step of the interrupted thermal treatments.

- By introducing longer oxidation treatment times during the continuous isothermal treatments similar hardening to that of the interrupted thermal treatment was achieved.

(ii) Cyclic isothermal treatments which cycle between step 1 and step 2 at constant temperature was introduced and it was speculated made that these treatments would produce higher boost diffusion hardening than the interrupted thermal OBDH treatments. The reason for this speculation being that a greater oxygen reservoir would accumulate during the cyclic oxidation steps than during one continuous step. It was also expected that greater interface integrity would be achieved during the formation of thinner oxide layers. Strain at the interface is caused by increased oxide layer thickness which these thin oxide layers would limit.

- Very little difference was found between the hardening during the cyclic isothermal and interrupted thermal treatments.

- Cyclic isothermal treatments are the most efficient in achieving appropriate boost diffusion hardening compared to interrupted thermal treatments.

(iii) To determine whether high vacuum is necessary for boost diffusion to occur the boost diffusion step was conducted under two different oxygen free environments: high vacuum and argon gas. Consequently no oxygen would be present at the oxide surface during step 2.

- Appropriate boost diffusion can be achieved in either oxygen free environment: high vacuum is therefore not required for boost diffusion to occur.

(iv) To determine the role of nitrogen in the OBDH process hardening results were compared for treatments during which the oxidation medium utilised was pure oxygen to those of treatments that utilised a mixture of oxygen and nitrogen as oxidation medium.

- Boost diffusion hardening is limited if nitrogen was present during step 1 of the OBDH process.

Further refinements of the OBDH process were made to the oxidation step by determining the optimum treatment time and temperature for the oxidation step and by using different oxidation mediums and introducing them through different gas flow methods into the furnace chamber.

- After 30 minutes of oxidation at 850^{o}C an oxide layer of 10 µm thick with good adherence to the underlying metal forms under pulsed oxygen conditions.

- Stratification of the oxide layer and separation at the interface occurs during cooling if the oxide layer is too thick. This occurs if the oxidation treatment time is longer than 30 minutes.

- Optimum boost diffusion during step 2 can be achieved regardless of the diffusion hardening that occurred during step 1.

Through the refinement of the OBDH process a clear understanding of the boost diffusion hardening mechanism was gained. During the first step oxygen diffusion movement results in the formation of a TiO_2 layer through the transformation of oxygen rich titanium metal. During the second step of the OBDH process continued diffusion movement down the oxygen concentration gradient results in a drop in oxygen concentration in titanium metal which causes the dissociation of oxygen out of titanium oxide. This dissociation actively decomposes the oxide layer and results of the transformation of TiO_2 into α titanium metal.

- TiO_2 formation occurs during step 1 through a nucleation and grain growth mechanism and starts at the metal surface continuing into the metal.

- During step 1 the formation of a graded zone (intermediate oxide layer) occurs between the TiO_2 and the underlying titanium metal.

- Transformation of titanium oxide occurs through the nucleation and grain growth of new α titanium grains at the interface as the decomposition of the oxide continues toward the surface during step 2.

- Grain growth of the α titanium metal grains occurs during step 2. Grain refinement of the titanium metal grains below the initial interface position was found although the mechanism for this refinement is not known.

- The occurrence of β grains increases with the decrease of oxygen content until the normalised a/β microstructure is found. Oxygen is a strong α grain stabiliser. In high oxygen concentration regions β grains transform into stable α grains.

6 FUTURE WORK

The following recommendations are offered for further refinement and understanding of the OBDH process:

- The mechanism which causes grain refinement of the α titanium metal below the old interface position must be identified.

- Analysis of the intermediate or sub-oxide layer should be conducted to determine the composition of the layer.

- Specimens should be coated before they are cut and set in resin. This would keep the oxide layer in tact during preparation for both hardness and microscopy. The oxide layer and sometimes some underlying material was pulled off from the specimen when it was removed from resin and during cutting of the specimen.

- The cyclic isothermal treatments should be conducted at 750^{o}C to see whether the same hardening can be achieved while limiting grain growth during the OBDH process.

7 REFERENCES

[1] Poggie, R.A., et al (1996) Oxygen diffusion Hardening of Ti-Nb-Zr Alloys, Materials and Manufacturing processes 11 No. 2 185-197

[2] Guleryus, H., (2005) Surface modification of a Ti-6Al-4V alloy by thermal oxidation, Surface & coatings Technology 192 164-170

[3] Zhang, Z., et al (2007) The effect of treatment condition on boost diffusion of thermally oxidised titanium alloy, Journal of Alloys and Compounds, 431 93-99

[4] Dong, H., et al (2000) Oxygen Boost Diffusion for the deep case hardening of titanium alloys, Materials Science and Engineering A280 303-310

[5] Luo, J., et al (2004) The computer simulation of the boost diffusion oxidation process for the deep-case hardening of titanium alloys, J. Phys. IV France 120 259-268

[6] Schuman, C., et al (2006) Modelling the oxygen diffusion profile in TA3V and T40 during heat treatment under air between 620 and 850 ^{o}C, Surface & Coatings Technology 200 4572-4578

[7] Lenarduzzi, E., et al (2003) Titanium Oxidation Treatment: Inhibiting Role of Nitrogen and Epitaxial Orientation Relations Evidenced by EBSD, Advanced Engineering Material 5 no 8 587-593

[8] Polmear, I.J. (2003) Light Alloys From Traditional Alloys to Nanocrystals, Fourth edition, Oxford:Elsevier/Butterworth-Heineman, 332

[9] Jackson, M., et al (2006) MATERIALS PERSPECTIVE, A review of advances in processing and metallurgy of titanium alloys, Materials Science and technology 22, no 8, 881-886

[10] Steven Yu, 3M Company, Corrosion resistance of Titanium Alloys, ASM Handbook, Volume 13A Corrosion: Fundemental Testing and Protection, 703-710

[11] Komotori, J., et al (2001) Corrosion response of surface engineered titanium alloys damaged by prior abrasion, Wear 251 1239-1249

[12] Komotori, J., et al (2007) The corrosion/wear mechanisms of Ti-6Al-4V alloy for different scratching rates, Wear, doi:10.1016/j.wear200611.025

[13] Shukla, A.K., et al (2005) Properties of passive film formed on Cp-Ti and Ti-6Al-4V and Ti-13,4Al-29Nb alloys in simulated human body conditions, Intermetallics 13 631-637

[14] Lopez, M.F., et al (2002) In vitro corrosion behaviour of titanium alloys without vanadium, Electrochimica Acta 47 1359-1364

[15] Choubey, A., et al (2004) Effect of replacement of V by Nb and Fe on the electrochemical and corrosion behaviour of Ti-6Al-4V in simulated physiological environment, Journal of Alloys and Compounds 381 288-249

[16] Tamilselvi, S., et al (2006) Corrosion behaviour of Ti-6Al-4V ELI alloys in the simulated body fluid solution by electrochemical impedance spectroscopy, Electrochimica Acta 52 839-846

[17] De Assis, S.L., et al (2006) Corrosion characterisation of titanium alloys by electrochemical techniques, Electrochemica Acta 51 1815-1819

[18] Khan, M.A., et al (1996) In-vitro corrosion and wear of titanium alloys in the biological environment, Biomaterials 17 2117-2126

[19] Keyser, C. (1959) Metallurgy Theories, Principles and Applications, Prentice-Hall Inc., Chapter 10, 313-316

[20] Boyer, R.R., (1996) An overview on the use of titanium in the aerospace industry, Materials Science and Engineering A213 103-114

[21] http://www.unitedtitanium.com/alloys/titanium/index.html

[22] http://asm.matweb.com/search/SpecificMaterial.asp?bassnum=MTP644

[23] http:// www.goodfellow.com/csp/active/gfhome.csp

[24] Metallography and microstructures, Metals Handbook Ninth Edition, American society for metals, Metals Park, Ohio, Volume 9, 458-469

[25] Brooks, C. (1982) Heat Treatment, Structure and Properties of Nonferrous Alloys, American Society fo Metals, Metal Park, Ohio, Chapter 9, 361-376

[26] Porter, D.A., and Easterling, K.E. (1996) Phase Transformation in Metals and Alloys, Second edition, Chapman and Hall, University and Professional division, Chapter 2, 61-107

[27] Januszewicz, B., et al (2006) The glow discharge plasma influence on the oxide layer and diffusion zone formation during process of thermal oxidation of titanium and its alloys, Vacuum 81 215-220

[28] Borgioli, F., et al (2004) Glow discharge and furnace treatments of Ti-6Al-4V, Surface and Coatings Technology 184 255-262

[29] Cai, Z., et al (2003) Electrochemical characterisation of cast titanium alloys, Biomaterials 24 213-218

[30] Koike, M., et al (2003) Corrosion behaviour of cast titanium with reduced surface reaction layer made by a face coating method, Biomaterials 24 4541-4549

[31] Song, H. et al., Surf. Coat. Technol. (2006), doi:10.1016/j.surfcoat.2006.11.22

[32] Borgioli, F., et al (2001) Air treatment of pure titanium by furnace and glow discharge, Surfaces and Coatings technology 141 103-107

[33] Chandler, H. (1998) Metallurgy for the non-Metallurgist, ASM International, The Materials Information Society, Chapter 6, 113-114

[34] Wang, R., et al (1997) Oxidation behavior of surface-modified titanium for titanium-ceramic restorations, The Journal of Prosthetic Dentistry 7 423-434

[35] Hirth, J.P., Mitchell T.E., The role of interface structure in oxidation reactions, Acta Mater (2008), doi:10.1016/j.actamat.2008.07.058

[36] Cumago, S., Surface Modifications of titanium-based Alloys, MSc Thesis, Centre for materials engineering. University of Cape Town. 2007

[37] Struers Application Guide for Hot Mounting

[38] Vander Voort, G.F., Van Geertruyden W., "Specimen Preparation for Electron Backscattered Diffraction", McGraw-Hill Book company Table 8, p23

Appendix A

Machine drawings for high vacuum system components and the turbomolecular pump stand.

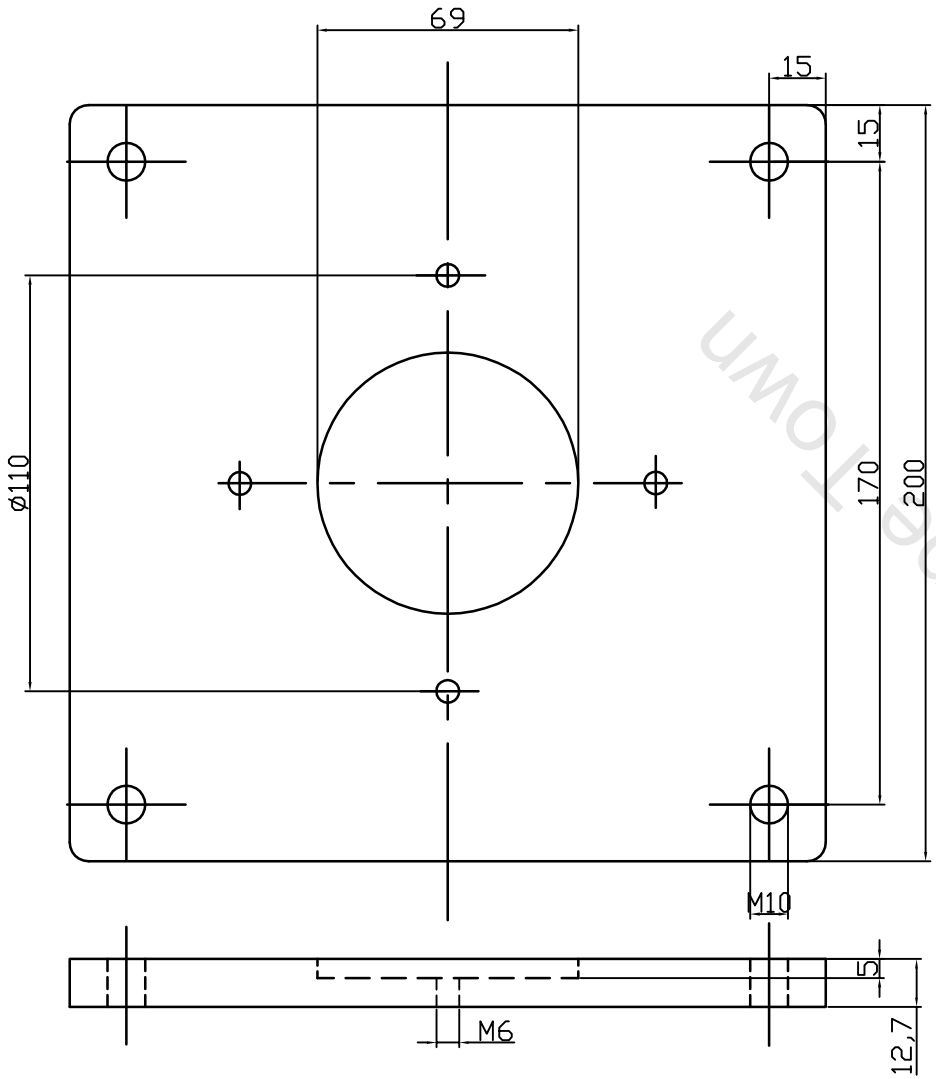

1

Al6061 plate

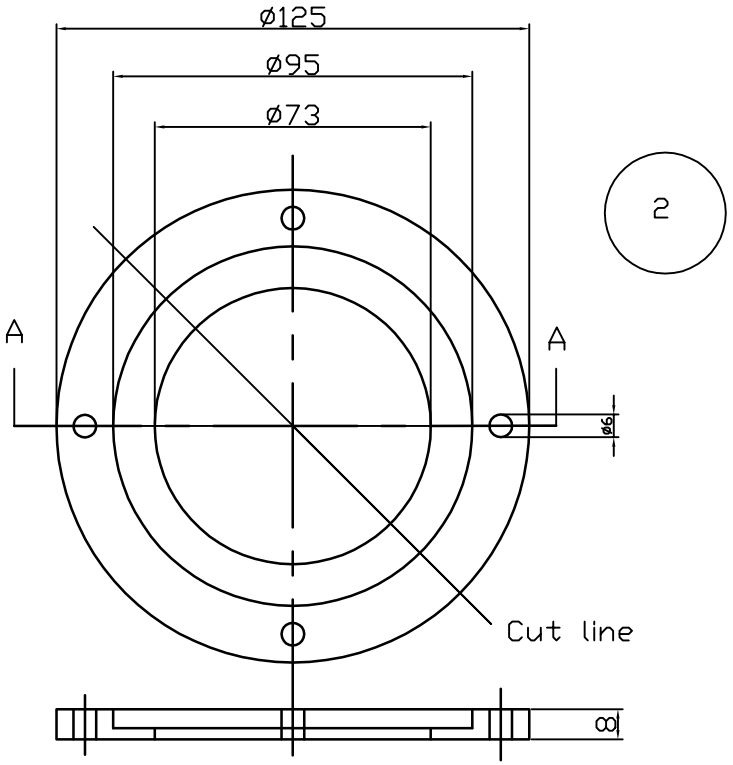

2

View AA

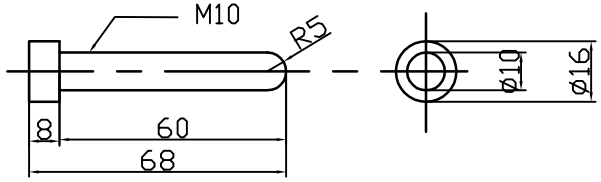

3

QTY	ITEM	DESCRIPTION	MATERIAL	PT NO.
4	Fasteners	M6 Hex Cap	Stainless Steel	
4	FEET	M10 Knurl Finish	Stainless Steel	3
1	CLAMP	Cut on cut line	Al6061 plate	2
1	PLATE		Al6061 plate	1

CENTRE FOR MATERIALS ENGINEERING

TITLE: Turbo pump stand

DRAWN BY: Liezl

SUPERVISOR SIGNATURE:

SCALE: 1 : 2

DATE: January 2008

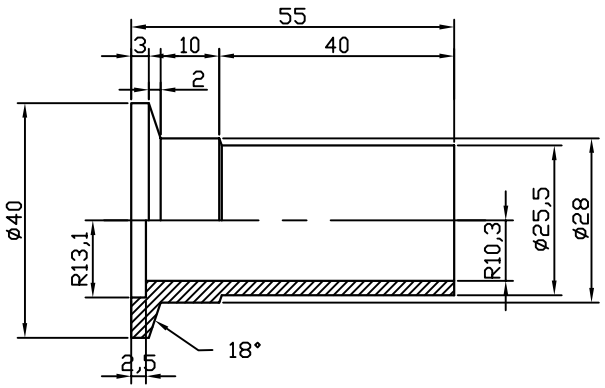

1

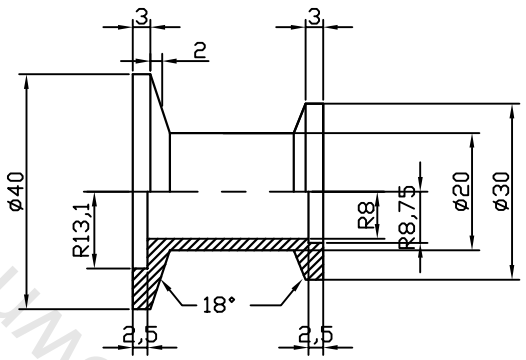

2

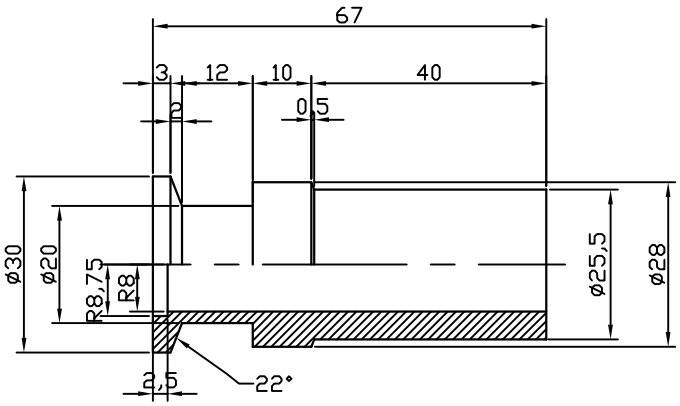

3

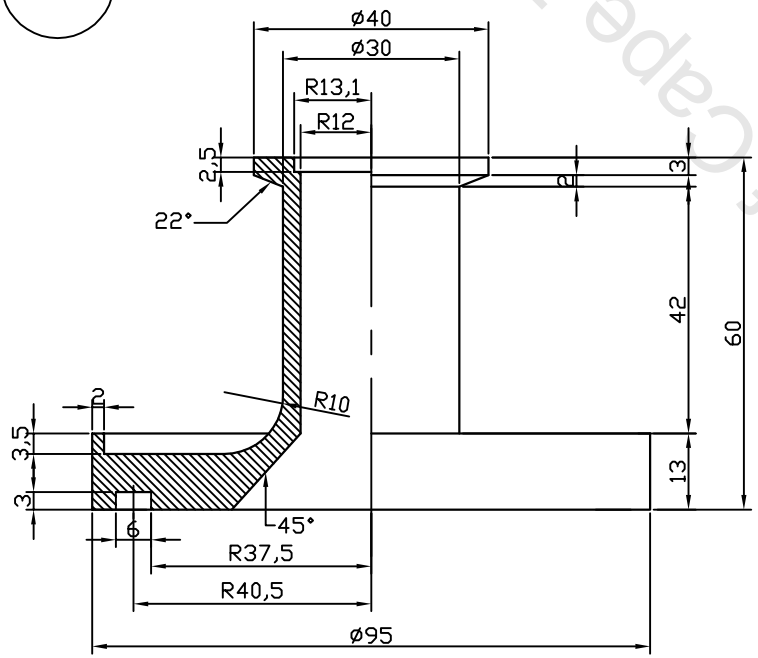

4

all parts made of bulk standard Aluminium

1	REDUCTOR	ID45.8mm to ID17.5mm	4
1	PIPE CONNECTER	ID17.5mm press fit	3
1	REDUCTOR	ID26mm to ID17.5mm	2
1	PIPE CONNECTER	ID 26 mm	1
QTY	ITEM	DESCRIPTION	PT NO.

CENTRE FOR MATERIALS ENGINEERING

TITLE: Vacuum fittings

DRAWN BY: Liezl

SUPERVISOR SIGNATURE:

SCALE: not to scale

DATE: January 2008